# A SOS in regulation of the SOS/ RAS positive feedback loop as identified by using single-molecule analysis in living cells

# 生細胞内の一分子計測に基づく、SOS/RAS positive feedback loop における調節因子としての SOS の機能の提案

**Special Research Promotion Group**

**Graduate School of Frontier Biosciences**

**Osaka University**

**Yuki Nakamura**

**Abstract**

The small GTPase RAS is a hub protein in signal transduction pathway. The input signals to the cell are integrated and divaricated by RAS, resulting in the differentiation, proliferation and survival in cells. To understand the regulation of cell response, the mechanism of RAS for processing multiple signals has to be clarified. The RAS bound to GDP is inactive and GTP bound RAS is in an active state. But, the GDP/GTP exchange rate in RAS is too slow to be triggered by signal-dependent activation. To activate RAS with a signal, the nucleotide exchange factor is required. Son of Sevenless (SOS) is one of RAS nucleotide exchange factors and activates RAS with epidermal growth factor (EGF). To understand signal-dependent RAS activation, the mechanism of RAS activation by SOS must be identified. So, the aim of this study is clarification of RAS activation mechanism caused by SOS. It is known that the RAS activation by SOS is affected by SOS-mediated RAS positive feedback. However, it is unknown whether SOS/RAS positive feedback functions in living cells or not, and how the positive feedback is regulated.

To solve the problems, this study observed Halo-SOS stained with tetramethyl rhodamine (TMR) in living HeLa cells by using total internal reflection fluorescence microscopy. Accordingly, it was revealed that SOS-mediated positive feedback has a positive role in living cells. And the mechanism of SOS/RAS positive feedback is that production of Intermediate state (I state), which is one of association state on the plasma membrane, induces long dwell time of SOS molecules that increases the number of molecules interacting with RAS-GTP at later stage. Additionally, it was suggested that the interactions between SOS domains regulates the fraction of I state precisely. These results indicated that the orientation and distance between domains regulates the RAS positive feedback.

Noonan syndrome (NS) is a congenital hereditary disorder with developmental and cardiac diseases. The 10-17% of NS patients has mutations in SOS. The NS mutations are identified in various SOS domains. The reports in which mutations in domains that do not interact with RAS were identified in NS patients support my suggestion that interaction of SOS domains regulates SOS/RAS positive feedback. And so, I examined whether NS mutants have abnormal molecular dynamics and different positive feedback response. By using single molecule analysis, it was revealed that NS mutants had abnormal affinity for the membrane in common but the molecular mechanism causing the abnormal affinity was different for each NS mutants. So, NS mutants could be classified from the view of SOS/RAS positive

feedback. The study shows the possibility in which the modulation of the interaction between SOS domains can control RAS activity. Additionally, it is suggested that the switching of SOS dynamics by conformational change functions well, when G domain of SOS has applicable affinity for the membrane. This suggestion shows the possibility that regulating mechanism of RAS positive feedback by interaction between SOS domains controls RAS activation when G domain has adequate affinity for the membrane. It is known that various proteins bind to the domains of SOS in living cells. By the interaction of SOS domains, which is regulated by other proteins binding to various domains of SOS, the SOS/RAS feedback response might be modulated. This study shows that SOS/RAS positive feedback is regulated by concerted interaction between SOS domains in living cells. It contributes to the clarification of RAS activation mechanism.

**INDEX**

# Chapter I

## 1. General introduction

## 1.1. Role of RAS and RAS-MAPK in cells

The study of small GTPase RAS started in 1964, and reports about RAS cancer pathogenesis advanced RAS study rapidly [Harvey *et al.,* 1964; Der *et al.,* 1982; Parada *et al.,* 1982; Santos *et al.,* 1982]. In 1982, it was reported that excess RAS activation by single mutation caused tumor [Reddy *et al.,* 1982]. In different tissues, various RAS (called as H-RAS, K-RAS, N-RAS and R-RAS) were identified [Kirsten *et al.,* 1967; Shimizu *et al.,* 1983]. Then in the 1990s, the first RAS guanine nucleotide exchange factor (GEF) and RAS effector were identified [Karnoub *et al.,* 2008]. A lot of studies in connection with RAS have been reported.

In cells, RAS has various input signals and conveys these signals to various effector proteins. It was revealed that EGF signal network including RAS, formed shape of a bow tie [Oda *et al.,* 2005] (Fig. 1.1). This structure of network suggests that input singles are branched and integrated in RAS. So RAS is a hub protein in cells and governs cell fate such as proliferation, survival, migration, apoptosis, endocytosis and adhesion [Vojtek *et al.,* 1998]. These reports suggest that activation of RAS has to be regulated precisely. RAS is converted to the active form by binding to GTP and to inactive form by combining with GDP. But transition rates between these two states are quite low [Margarit *et al.,* 2003]. So, in cells, RAS GEF and RAS GTPase activation protein (RAS GAP) promote the release of GDP from RAS and the hydrolysis of GTP [Boguski *et al.,* 1993]. The signal dependent activation of RAS is regulated by these proteins. Thus, to reveal the regulation of RAS activation which is necessary to adequate cell response, the GEF and GAP activities need to be clear in cells.

This study focused on the GEF. Son of Sevenless is one of the GEF and regulates RAS activation with epidermal growth factor (EGF) stimulation. The crystal structure of RAS

binding to SOS revealed that the binding induces release of GTP from RAS [Boriack-Sjodin *et al.,* 1998]. With EGF stimulation, the EGF receptor (EGFR), one of receptor tyrosine kinases (RTKs), binds to EGF and dimerizes and is phosphorylated [reviewed in Heldin, 1995 and Weiss and Schlessinger, 1998]. Various cytosol proteins like GRB2, Shc and PLC-γ, bind to the phosphorylation site of EGFR and convey extracellular single to the cytosol. In the resting cells, SOS forms a complex with GRB2 in the cytosol. With EGF stimulation, SOS binds through GRB2 to phosphorylated EGFR and activates RAS on the plasma membrane (Fig. 1.2). Activated RAS induces activation of effector proteins such as RAF. Then, the signal is transmitted through MEK to ERK (also called as MAPK) and conveyed to the cell nucleus.

Patients suffering from Noonan syndrome (NS) have a mutation in genes involved with RAS MAPK signal pathway. NS is a congenital and genetic disorder with cardiac and developmental diseases. In this disease, various phenotypes such as short stature, characteristic facies, learning problems and leukemia predisposition are observed [Tartaglia and Gelb, 2005] (Fig. 1.3). In Noonan syndrome patients, mutations of Shp2, SOS and RAS MAPK protein were identified. The patients with mutations in SOS and RAS account for 10-17% and 13% of Noonan syndrome patients, respectively [Zenker *et al.,* 2006 and Roberts *et al.,* 2007]. Because RAS-MAPK proteins have crucial role for cell response, single mutation of one protein causes various phenotype. These various phenotypes disturb the study of basal treatment for NS. So, patients with Noonan syndrome are provided with only symptomatic treatment at present. Therefore, the clarification of RAS activation mechanism is significantly important to the establishment of basal therapy for NS.

## 1.2. General introduction about Son of Sevenless (SOS)

The crystal structure of RAS with SOS revealed that SOS bound to RAS at the periphery of nucleotide binding site in RAS [Boriack-Sjodin *et al.,* 1998; Hall *et al.*, 2001]. At the SOS-RAS complex, the switch I is uncoupled from the switch II in RAS, inducing a conformational change. This structural alteration of RAS, which is caused by SOS, induces release of GTP and association with GDP. Using this mechanism, SOS functions as RAS GEF. On the plasma membrane, SOS activates RAS dependently on EGF stimulation [Aronheim *et al.,* 1994].

SOS has six domains. The translocation of SOS from the cytosol to the plasma membrane is derived from the function of five domains, which associates with the plasma membrane. These domains have different functions, respectively (Fig. 1.4). The GRB2 binding domain (G domain) at C terminus of SOS has four proline-rich motifs that bind to SH3 domain in GRB2. In resting cells, the G domain binds to GRB2 in cytosol. With EGF stimulation, the G domain of SOS associates with phosphorylated EGFR through GRB2, inducing signal dependent response. Once the EGF signal is conveyed to ERK via RAS, activated ERK phosphorylates four residues (S1132、S1167、S1178、S1193) of G domain in SOS [Zarich *et al.,* 2006; Corbalan-Garcia *et al.,* 1996]. Because these residues are located in proline-rich motif, this phosphorylation by ERK represses interaction between G domain and Grb2. This reaction is known as negative feedback of SOS caused by ERK. And residues S1134 and S1161 in G domain are also phosphorylated by ribosomal S6 kinase (RISK) that is activated by ERK. These phosphorylated residues form 14-3-3 docking site, inducing down-regulation of ERK activation [Saha *et al.,* 2012]. Thus, SOS activation is regulated by ERK and RISK negatively at G domain (Fig. 1.5). The nucleotide exchange reaction of RAS is performed at catalytic domain of SOS called

as Cdc25. On the plasma membrane, this domain interacts with inactivated RAS, which binds to GDP. The REM domain interacts with both activated RAS (RAS-GTP) and inactivated RAS (RAS-GDP). PH domain binds to phosphatidic acid (PA) and phosphatidylinositol 4,5-bisposphate ($PIP_2$), that is one of the components of the plasma membrane. H domain is located in N terminus of SOS and has a histone-like motif [Sondermann *et al*., 2003]. Additionally, H domain binds to the plasma membrane by the distribution of electric charge in H domain [Gureasko *et al*., 2010].

By crystal structure analysis, it was revealed that SOS binds to a couple of RAS, and the association of REM domain with RAS-GTP causes the RAS feedback activation [Margarit *et al*., 2003].The result that increase of RAS-GTP causes an elevation of GEF activity in SOS indicated that affinity of REM domain for RAS-GTP is higher than RAS-GDP. To inhibit the feedback response in resting cells, it was suggested that SOS forms autoinhibition state [Sondermann *et al.*, 2004, 2005]. In this state, REM domain is disturbed by DH domain, inhibiting the interaction between REM domain and RAS. And the binding of H domain to the helical linker (HL), which locates between DH and PH domains, stabilizes this autoinhibition state (Fig. 1.4). *In vitro* studies suggested that the release of this interaction between H domain and HL induces the association of REM domain in SOS and RAS, amplifying the input signal with extracellular stimulation. In R552G mutants found in patients with NS, it is known that the interaction between H domain and HL is inhibited, supporting this suggestion [Sondermann *et al.*, 2005]. But, it is still unclear whether the positive feedback functions in living cells, and if so, how positive feedback is regulated in living cells.

Mutation in SOS identified in Noonan syndrome patients is located in various domains [Tartaglia *et al.*, 2007; Narumi *et al.*, 2008; Lepri *et al.*, 2011] (Fig. 1.6). A

number of mutations were identified not only in Cdc25 domain and REM domain but also DH and HL. In view of location in crystal structure, majority of these mutations probably alter not the interaction of SOS with RAS but the interaction between SOS domains. But it is unknown how the interactions between SOS domains affect SOS activity and SOS/RAS positive feedback, which is important to RAS activation.

### 1.3. Purpose of this study

To understand the adequate cell response, and to propose the fundamental therapeutic method for Noonan syndrome, the mechanism of RAS activation has to be clarified. Many in vitro studies reported the activation of RAS mediated by SOS. But these studies were not able to detect the subtle change of SOS dynamics with signals. Thus, the aim of this study is clarification of signal-dependent activation mechanism of RAS by the analysis of SOS molecular dynamics in living cells by using single molecule imaging. And so, I focused on detailed analysis of SOS-mediated RAS positive feedback, which is important to the RAS activation, and examined the function of SOS as regulator for SOS/RAS positive feedback.

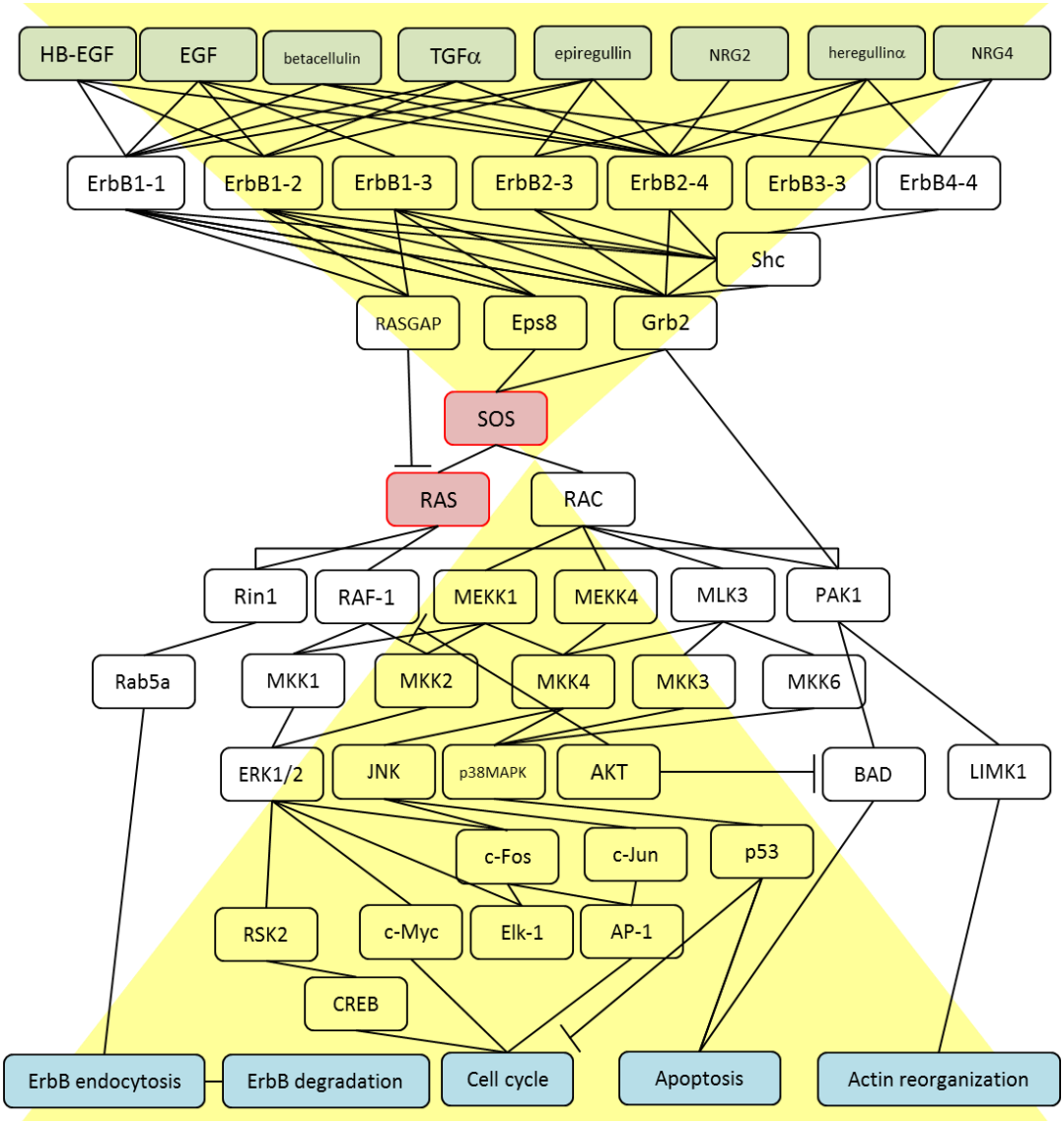


**Figure 1.1. The map of EGF signal network**

The signal pathway of ErbB family, which involves in SOS and RAS is shown [Oda *et al.*, 2005]. The shape of this EGF signal network is like a bow tie (yellow area). Multiple extracellular signals such as EGF, TGFα and NRG are transmitted to SOS and RAS. Appropriate cell response is selected from multiple options such as cell cycle, apoptosis and actin reorganization. SOS and RAS are located on the knot of the bow tie. The integration and divarication of signals might be performed around RAS.

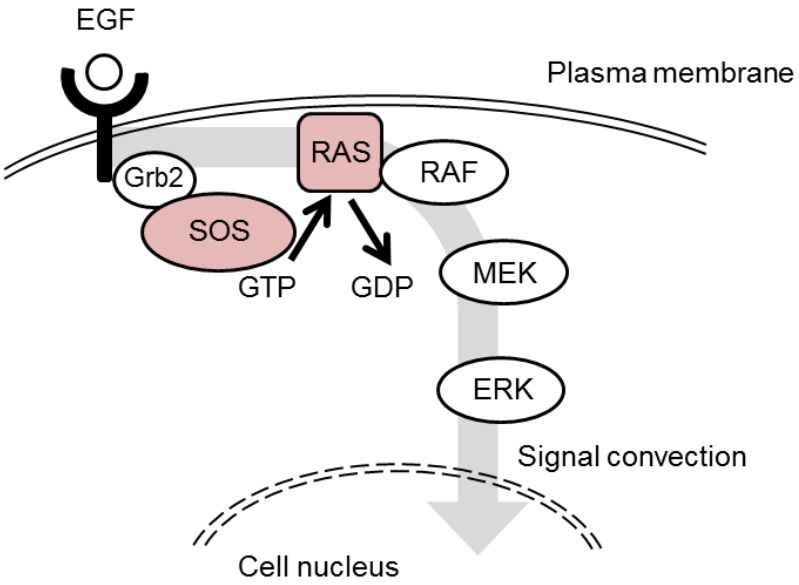


**Figure 1.2. Signal pathway with EGF stimulation**

EGF-binding EGFR dimerizes and is phosphorylated. SOS which is bound to Grb2 associates with phosphorylated EGFR via Grb2. Then, SOS activates RAS on the membrane. Activated RAS interacts with RAF on the membrane. Thus, EGF signal migrates to cell nucleus through the membrane and cytosol.

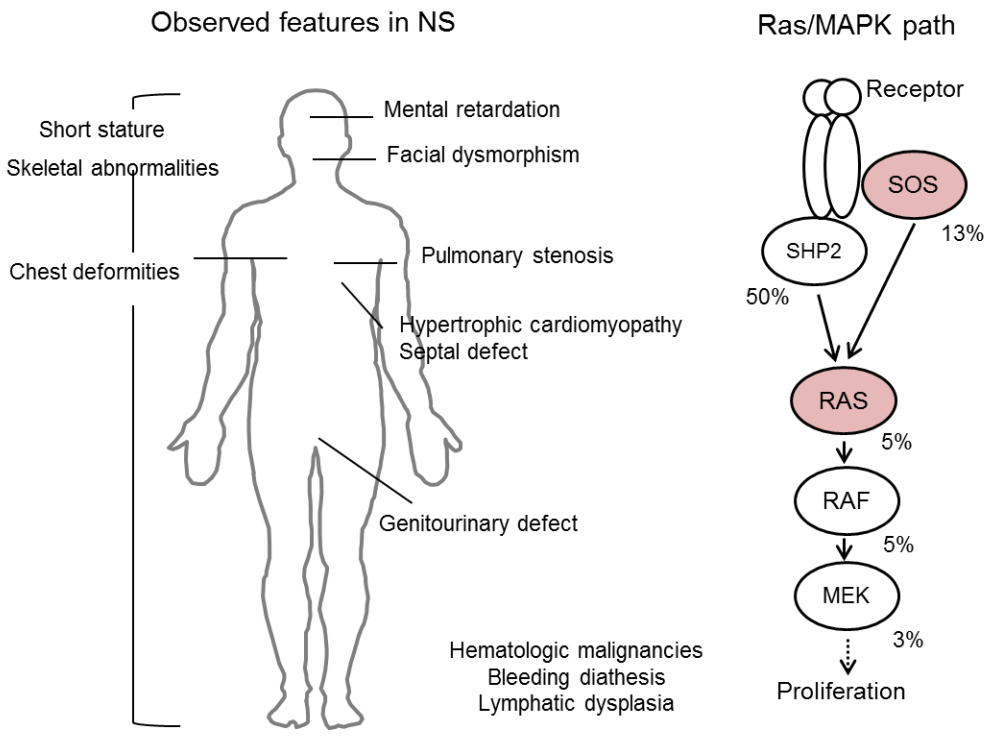


**Figure 1.3. Feature of Noonan syndrome**

Typical symptom in Noonan Syndrome patients are described (left). NS is congenital inherited disease with various symptoms like cardiac disorder and mental retardation. Mutations in the proteins involved in RAS MAPK pathway were identified in patients with NS (right). Mutation in SOS accounted for 13% among all patients with NS.

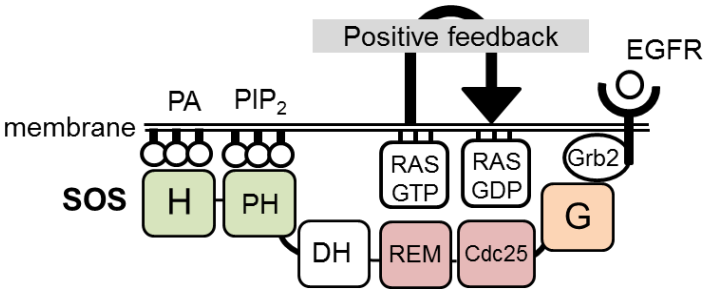


**Figure 1.4. Structure diagram of SOS**

SOS has five domains which associate with the plasma membrane. H domain binds to PA electrically. PH domain associates with PA and $PIP_2$. REM domain interacts with RAS-GTP (active RAS). Cdc25 domain interacts with RAS-GDP (inactive RAS) and exchanges GDP to GTP. G domain associates with phosphorylated EGFR through GRB2.

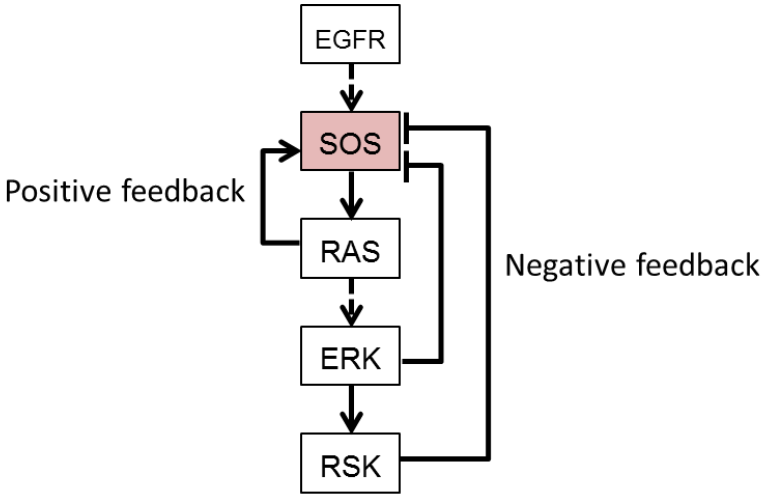


**Figure 1.5. Network diagram around SOS**

SOS activity is upregulated by activated RAS, leading to RAS positive feedback. And SOS activity is inhibited by ERK and RSK, resulting in negative feedback. Dashed line shows indirect interaction.

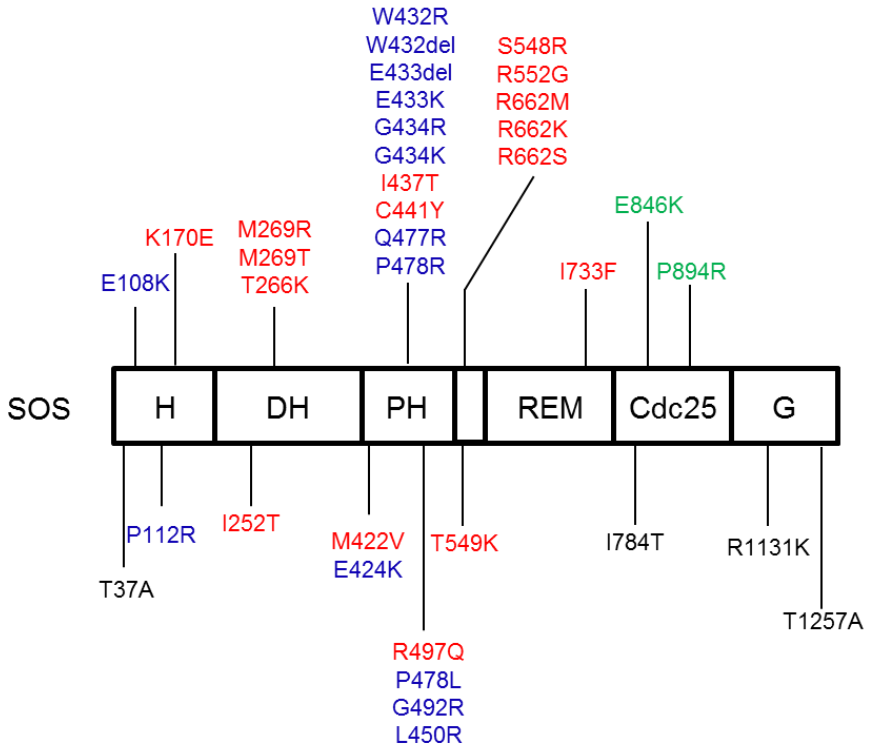


**Figure 1.6. SOS mutation site identified in the Noonan syndrome patients**

Mutation site identified in NS patients is described. Difference of color shows abnormal function predicted by crystal structure. Blue indicates mutations which have strong association with PA and $PIP_2$. Green shows the mutations promote conformation change of Cdc25 domain. And red indicates the mutations drive conformation change of autoinhibition release. Black shows the mutations have unknown function.

# Chapter II

## 2. Switching of the positive feedback for RAS activation by a concerted function of SOS membrane association domains

## 2.1. Introduction

SOS consists of six domains which has specific function respectively (Fig. 2.1) and has five domains which interact with the plasma membrane: H, PH, REM, Cdc25 and G.

Recent *in vitro* study has suggested that positive feedback regulates RAS activation mediated by SOS [Margarit *et al.,* 2003], i.e., the interaction between REM domain of SOS and RAS-GTP allosterically promotes the nucleotide exchange of RAS-GDP at catalytic site in Cdc25 domain (Fig. 2.2). An *in vitro* study demonstrated that in the presence of $RAS^{Y64A}$-GTP, mutants of SOS in the REM domain (L687E/R688A and W729E) lowered the nucleotide dissociation rate of RAS by a factor of ten relative to that of the wild-type [ Hall *et al.,* 2001]. $RAS^{Y64A}$-GTP binds to the allosteric (positive feedback) site in the wild-type REM domain but not to the catalytic site. A combination of *in vitro* and *in silico* study suggested that positive feedback mechanism maintains RAS activation, eliciting memory of antigen in lymphocyte [Das *et al.,* 2009]. It is thought that in the inactive conformation of SOS, association of RAS-GTP with REM domain is disturbed by steric hindrance attributable to the interaction between the DH and REM domains. Additionally, an intramolecular interaction between H domain and HL is thought to be important to maintain the inactive autoinhibited conformation of SOS, because a mutation in the helical linker (R552G) increases the nucleotide dissociation rate of RAS [Gureasko *et al.,* 2010] and because the mutated helical linker does not interact with the H domain [Sondermann *et al.,* 2005]. This gain-of-function mutant was found in Noonan syndrome patients. A previous study has shown that RAS is excessively activated by this mutation when cells are stimulated with epidermal growth factor (EGF) [Roberts *et*

*al.,* 2007]. It has been suggested that the membrane recruitment of H domain is coupled to the release of autoinhibition. Thus, coordination between SOS domains seems to be required to activate SOS molecules and regulate the positive feedback of RAS activation.

These results were mostly obtained through in vitro biochemical experiments and X-ray crystallographic studies of the segments of SOS and RAS. The GEF activity of SOS molecule with a truncation of the G-domain was analyzed in a reconstructed system using fluorescence microscopy [Iversen *et al.,* 2014]. However, it remains unclear how the positive feedback mechanism functions, and especially, how the positive feedback is regulated in living cells. In this study, I observed single-molecules of SOS on the plasma membrane of living HeLa cells to determine the dynamics and kinetics of SOS behaviors in response to EGF stimulation. Single-molecule imaging is a useful technique for tracking the dynamics of a small number of molecules [Matsuoka *et al.,* 2006] and analyzing the kinetics of molecular interactions [Hibino *et al.,* 2011; Hiroshima *et al.,* 2012] in living cells. Comparing the behaviors of wild-type and mutant of SOS molecules, it was found that concerted function of the SOS membrane association domains is necessary to switch on the SOS/RAS positive feedback, which crucially regulates the activation of RAS in living cells.

## 2.2. Material and methods

### 2.2.1. Construction of plasmids

The Halo7 plasmid vector was constructed by exchanging EGFP in pEGFP-C2 vector (#6083-1, BD Biosciences Clontech.) for Halo7 (Fig. 2.3). The pEGFP-C2 vector is derived from the FN19K HaloTag T7 SP6 Flexi Vector (Promega)

(Fig. 2.4). Halo7-SOS cDNA was constructed by inserting the hSOS1 fragment from pCGN-HAhSos1 [Chardin *et al.*, 1993] into the Halo7 vector with PCR. SOS point mutants were constructed by directly introducing mutations into Halo 7-SOS using the PrimeSTAR® Max DNA Polymerase (Takara) and QuikChange Lightning Site-Directed Mutagenesis Kit (Agilent Technologies). The truncation mutants of SOS were cloned into Halo7-SOS with the appropriate primer sets. The domain structure of wild-type and mutant SOS molecules are shown in Figure 2.1. The construction of GFP-RAF cDNA has been described in Hibino *et al.*, 2003.

### 2.2.2. Cell preparation

**Culture condition**

HeLa cells were maintained in Dulbecco's modified Eagle's medium (DMEM), supplemented with 10% fetal bovine serum (Hyclone®), at 37°C under 5% $CO_2$. Aseptic treatment was performed in clean bench (SANYO). When HeLa cells were passed, the cells were detached from dish by addition of 0.0025 g/ml trypsin.

**Transfection condition**

Plasmids were introduced by using Lipofectamine® LTX with Plus™ Regent (Invitrogen) into HeLa cells which were incubated on cover glasses. The 2 μM Plus reagent and 2 μg plasmid were diluted with 250 ml of Opti-mem® I (Reduced Serum Medium 1X, GIBCO) and incubated at room temperature for five minutes. Then, 5 μl Lipofectamine LTX was mixed into this compound liquid and incubated at room temperature for 15 minutes. This compound liquid was mixed into HeLa cell. After 3 hours, the medium was exchanged.

**Wash of cover glasses**

The 25 mm round cover glasses (MATSUNAMI MICRO COVER GLASS, MATSUNAMI GLASS IND) were washed with Milli-Q water over ten times and rinsed overnight in concentrated sulfuric acid. Then, these cover glasses were washed in Milli-Q water and autoclaved (TOMY) at 120°C. These cover glasses were stored in Milli-Q water.

**TMR staining**

After transfection, cells were incubated in Eagle's MEM 3 (NISSUI PHARMACEUTICAL CO., LTD.) without pH indicator, supplemented with 1% BSA (Albumin, from bovine serum, SIGMA). The cells were incubated for 15 min with 100nM HaloTag® TMR Ligand (Promega) in MEM (Fig. 2.5). And the cells were washed with HBSS twice with MEM once, followed by a 15 min incubation in MEM supplemented with 1 % BSA. Then, the cells were washed in MEM supplemented with 1 % BSA.

**Observation condition**

After TMR staining, HeLa cells on the cover glass were held on Attofluor® cell chamber (invitrogen) in 900 μl MEM, supplemented with 1% BSA and 5 mM PIPES (pH 7.5) (DOJINDO). The final concentration of EGF was 100 ng/ml (Recombinant Murine EGF, PEPROTECH). The fluorescence images of SOS were acquired before and at 3 min and 8 min after EGF stimulation at 25°C.

**Methanol fixation of cells**

Cells were washed with HBSS (Sigma) after transfection and fixed with methanol at room temperature for 5 minutes. After removal of methanol, cells were washed in HBSS.

### 2.2.3 Immunoblotting analysis

Hela cells which were transfected with plasmids encoding SOS molecules using Lipofectamine® LTX with Plus$^{TM}$ Regent, and incubated overnight in MEM, supplemented with 1% BSA. The cells were washed twice with HBSS and harvested in SDS solubilization buffer. The proteins in the cell lysates were separated according to their molecular sizes on 10% or 8% polyacrylamide gels, and transferred to polyvinylidene difluoride membranes (BD Biosciences). The membranes were incubated in 5% skim milk with anti-Halo-tag (anti-HaloTag® pAb; Promega) or anti-SOS1 (#5890; Cell Signaling), and a secondary antibody, which was conjugated with alkaline phosphatase (Vectastain ABC-AP Kit; Vector Laboratories). The membranes were stained using 5-bromo-4-chloro-3-indolyl phosphate/*p*-nitroblue tetrazolium chloride color development substrate (Promega).

### 2.2.4. Single-molecule imaging

**Microscope setting of single molecule imaging**

Single molecules of Halo-SOS stained TMR (TMR-SOS) were observed in living HeLa cells using a home-made total internal reflection microscope (TIRFM) based on an inverted microscope (IX81, Olympus) (Fig. 2.6) [Hibino et al.,2009]. The molecules of Halo-SOS were illuminated with a 555 nm solid laser (GCL-075-555, CrystaLaser) through an objective (PlanApo 60× NA=1.49, Olympus). Fluorescence images of single molecules were acquired at an emission wavelength of 560–680nm using an electron-multiplying CCD camera (ImagEM, Hamamatsu Photonics), at a frame rate of 20 $s^{-1}$.

**W view system**

To observe TMR-SOS and GFP-RAF simultaneously, W view system was used (TE200-E, Nikon) (Fig. 2.7). TMR-SOS and GFP-RAF were illuminated with a 559 nm and 488 nm solid laser (WS-0559-050-A-A-E-R001, NTT Electronics Corporation, SHAPPHIRE 488-200, COHERENT). To separate these lasers, a dichroic mirror (493/574) was used. Fluorescence images were acquired at an emission wavelength of 585/40 nm (GFP) and 679/29 nm (Halo7).

**Image processing**

Acquired images were averaged each 3 pixels. Background noise was subtracted from these images.

### 2.2.5. Detection of single molecules conjugated with TMR

The photobleaching step size and fluorescence intensities in living cells were compared with methanol-fixed cells to confirm the detection of single SOS molecules. To determine the intensities of single molecules, cells that expressed TMR-SOS were fixed with methanol, and the fluorescence intensities of individual TMR-SOS particles on the plasma membrane were measured immediately prior to the final photobleaching, which caused the particles to disappear (Fig. 2.8A). The intensity distribution fit well with a single Gaussian function:

$$y_i = A * \exp\left(-\frac{(x-\mu)^2}{2\sigma^2}\right)$$

Here, $\mu$ and $\sigma$ are the mean and standard deviation of the single-molecule fluorescence intensity. The estimated $\mu$ and $\sigma$ were 793 and 319 in arbitrary units respectively ($A$ = 24). Similarly, the intensity distribution of TMR-SOS measured in

living HeLa cells before EGF stimulation fit well with the single Gaussian function, providing best-fit values $\mu$, $\sigma$, and $A$ were 802, 223, and 34, respectively (Fig. 2.8B). The high agreement between these two $\mu$ values suggests that TMR-SOS molecules on the membrane were detected at single-molecule resolution in living HeLa cells.

To confirm the effect of nonspecific binding of TMR, cells with and without transfection of Halo-SOS were stained with TMR and observed by using TIRFM. There were few fluorescence particles in cells without transfection (Fig. 2.9). This data indicated that TMR stained Halo tag specifically.

### 2.2.6 Construction of kinetic models for SOS dissociation from the membrane

The dwell time distributions of single molecules of the G and H domains (Fig. 2.10) could be described with single exponential functions:

$$y_G = A_G * \exp(-k_{1r} - k_b)\, x$$

and $$y_H = A_H * \exp(-k_{2r} - k_b)\, x$$, respectively,

suggesting a single-step stochastic dissociation form membrane components. Here, $k_b$ is the rate constant for photobleaching. The value of $k_b$ was determined from time decays of TMR-SOS fluorescence in fixed cells (Fig. 2.11A), and TMR-conjugated EGFR fluorescence in living cells (Fig. 2.11B). Both measurements yielded $k_b$ =0.05 $s^{-1}$. By using this photobleaching rate constant ($k_b$), we estimated the dissociation rate constants of G domain ($k_{1r}$), caused by the dissociation of GRB2 form activated EGFR, and H domain ($k_{2r}$), from the membrane lipids, to be $k_{1r}$ = 1.5 $s^{-1}$ and $k_{2r}$ = 1.9 $s^{-1}$ (Fig. 2.10). The distributions of G and H domains did not change with time of EGF stimulation of the cells (Fig. 2.11CD), supporting the premise that the

dissociation rate constants are determined by the same components in the membrane at every stage of stimulation.

SOS has five putative membrane-binding domains (Fig. 1.4). I examined the domains of SOS that regulate the extension of its dwell times after cell stimulation (Fig. 2.12 and Fig. 2.1). Compared with the dwell times before stimulation, those of wild-type SOS (WT) molecules were extended after EGF stimulation for 3 min, and this extension was sustained until at least 8 min (Fig. 2.12A). In contrast, the dwell time distributions of the mutant truncated G and H domains (G(–) and H(–)) did not elongate after stimulation even at 3 min (Fig. 2.12BH). These data indicated that G domain and H domain contributed to dissociation of SOS from the plasma membrane. Thus, I constructed the dissociation kinetic models from the membrane including G and H domains (Fig. 2.13). For simplification, I also assumed that the G and H domains dissociated from the plasma membrane components independently.

The dwell time distribution in WT did not fit well with a double exponential function that means simple sum of the direct dissociations from the G and H states (Fig. 2.13A). A model that assumed direct transitions between the G and H states also failed (Fig. 2.13B). Therefore, I constructed the model which included an intermediate (I) state (Fig. 2.13C). The differential equations of the model are

$$\frac{dG(t)}{dt} = k_{2r} \cdot I(t) - (k_2 + k_{1r} + k_b) \cdot G(t),$$

$$\frac{dH(t)}{dt} = k_{1r} \cdot I(t) - (k_1 + k_{2r} + k_b) \cdot H(t),$$

$$\frac{dI(t)}{dt} = k_2 \cdot G(t) + k_1 \cdot H(t) - (k_{1\mathrm{r}} + k_{2r} + k_b) \cdot I(t),$$

Here, $k_1$ and $k_2$ are the association rate constants for the G and H domains from the H and G states, respectively. The values of $k_{1\mathrm{r}}$, $k_{2\mathrm{r}}$, and $k_{\mathrm{b}}$ are common to the

dissociation kinetics of the G and H domains mentioned above. $G(t)$, $H(t)$, and $I(t)$ are the possibilities with which the SOS molecules stay in each state. The initial conditions $G(0)$ and $H(0)$, ($G(0) + H(0) = 1$) were determined from the relative association rate constants of the H(–) and G(–) molecules (Fig. 2.14), and $I(0) = 0$. In the single-molecule dwell time measurements, we observed only dissociation process of SOS from the cell surface. Therefore, the kinetic model does not include associations of SOS from the cytoplasm to the cell surface.

The dwell-time distributions were fit with the function, $d\emptyset(t)/dt$, using the lsqcurvefit function in MATLAB, numerically solving the coupled differential equations with Ode45 solver in MATLAB. This model fitted the experimental distribution well (Fig. 2.13C).

### 2.2.7 Kinetic analysis

The detection and tracking of single molecules was performed by using in-house software [Hibino et al, 2003] and TrackMate [Jaqaman et al. 2008]. Curve fitting for the kinetic analysis were performed using Origin (Originlab) and Matlab (The MathWorks).

## 2.3. Result and discussion

### 2.3.1. Single molecule imaging of SOS dynamics

I observed TMR conjugated-Halo7-SOS (TMR-SOS) as single molecules on the plasma membrane in living HeLa cells by using TIRFM (Fig. 2.15A). On incubation of cells with the TMR ligand of Halo7, the association and dissociation of individual TMR particles with the plasma membrane were detected as the stepwise appearance and disappearance of fluorescence signals, respectively (Fig. 2.15B). The

fluorescence intensities of these particles were similar to the photobeaching step size of molecules that were fixed on the plasma membrane (Fig. 2.8A and Fig. 2.15B), and few fluorescence particles were observed in cells that lacked expression of Halo7-SOS under the same staining conditions with the TMR ligand (Fig. 2.9). In the Western blot analysis, the Halo-SOS expressed in HeLa cells displayed the expected molecular weight (Fig. 2.16A). The amounts of Halo-SOS in single cells were estimated relative to endogenous SOS expression, based on the staining intensities in the immunoblotting analysis and normalized to cell numbers and transfection efficiency (~45 % of cells). The amount of exogenously expressed Halo7-WT SOS per cell under our experimental conditions was approximately twice of endogenous SOS (Fig. 2.16B). Halo7-WT SOS and all Halo7-SOS mutants used in this study had the expected molecular weight when expressed in cells (Fig. 2.16CD). The expression levels of the point mutants were similar to that of WT SOS (Fig. 2.16C). These data indicated that behaviors of single SOS molecules were detected in living cells. These single molecules of SOS may be incorporated into clusters of SOS molecules [Sondermann *et al.*, 2007]. Small but significant amount of SOS molecules were transiently attached to the plasma membrane before the cells were stimulated with EGF. After stimulation, the density of SOS molecules on the plasma membrane increased, peaking at 3 min, and the increased density preserved, on average, until 8 min (Fig. 2.17A). The time course of SOS translocation was similar to that of RAS activation (Fig. 2.22). Thus, my single-molecule imaging data support the model in which SOS is expected to be recruited to the plasma membrane as a requirement of Ras activation [Aronheim *et al.*, 1994].

In addition to WT SOS, I examined a triplet mutant of SOS in the REM domain (L687E/R688A/W729E) and a single mutant (D140A) in the H domain (Fig. 2.1). The mutant SOS molecules were designated REM(–) and AI(–), respectively. It was reported that L687E/R688A and W729E abolished the positive feedback response in SOS-mediated RAS activation [Sondermann *et al.,* 2004]. In an earlier study, the D140A mutant disrupted the association between the HL and H domain [Sondermann *et al.,* 2005]. In crystal structure, D140A interacts with R552G in the HL. Thus, AI(–) is in the interaction between HL and H domain. Residue of D140A in SOS is conserved in many animal species, from *C. elegans* to humans [Sondermann *et al.,* 2003].

We compared the increase in the density of SOS molecules on the plasma membrane of individual cells at various times of stimulation with EGF (Fig. 2.17B). The densities of WT and REM(–) SOS molecules increased similarly after stimulation for 3 min. However, at 8 min, the average of increase in REM(–) was significantly less than that of WT. To detect the sustainability of SOS translocation, the distribution of SOS densities in individual cells at 8 versus 3 min is plotted in Figure 2.17C. Most cells experienced sustained translocation of WT-SOS molecules. However, the majority of cells showed transient translocation of REM(–). This result suggests that the interaction between the REM domain and RAS-GTP is required for the sustained translocation of SOS. The average increases in the density of AI(–) were modest at both 3 and 8 min (Fig. 2.17B). A population of cells showed sustained translocation of AI(–), but most exhibited transient (and weak) translocation (Fig. 2.17C). It is likely that the AI(–) mutation destabilizes the structure of SOS which is required for its normal association with the membrane components. These data

indicate that these mutants of SOS with defects in the positive feedback loop are also altered in the dynamics of membrane translocation, but the effects of mutations are not identical.

### 2.3.2. Interaction kinetics of SOS molecules with the plasma membrane

The density of SOS molecules on the plasma membrane is determined by the rate of association and dissociation. First, I measured the dwell time of single SOS molecules on the plasma membrane to determine the dissociation kinetics (Fig. 2.15B, Fig. 2.12ADH). WT and mutant SOS molecules dissociated from the plasma membrane faster than the photobleaching (Fig. 2.11AB), indicating rapid turnover of single-molecules of SOS. Turnover of single molecules was much faster than the dynamics of translocation, meaning that the accumulation of SOS on the plasma membrane is maintained as a dynamic equilibrium [Hibino *et al,* 2003]. Compared with the dwell times before EGF stimulation, those of WT molecules were extended after EGF stimulation for 3 min, and this extension was sustained until at least 8 min (Fig. 2.12A). A similar extension was observed for the dwell times of REM(–) at 3 min, but it was not sustained (Fig. 2.12D). The dwell times of AI(–) increased only slightly after EGF stimulation (Fig. 2.12H). As shown here, in addition to the translocation dynamics (Fig. 2.17.BC), the dwell times of single SOS molecules on the plasma membrane were affected by mutations in the domains responsible for the positive feedback reaction.

We examined the domains of SOS that regulate the extension of its dwell times after cell stimulation. SOS contains five putative membrane-binding domains. In addition to REM(–), I constructed four mutants of SOS corresponding to a loss of

function in each of the remaining membrane-binding domains (Fig. 2.1), and measured their dwell times (Fig. 2.12B-F). PH(–) and Cdc25(–) had dwell time distributions that were similar to that of WT both before and after EGF stimulation (Fig. 2.12CE). Cdc25(–) is inactive, but the activities of endogenous WT SOS could induce dwell time elongation of Cdc25(–). In contrast, the dwell time distributions of G(–) and H(–) did not increase after EGF stimulation even at 3 min (Fig. 2.12BF), indicating that these domains coordinate to extend the dwell time of SOS.

Next, I examined the association of SOS molecules by monitoring the appearance of the fluorescent particles on the plasma membrane from the cytoplasm (Fig. 2.18A). To determine the relative association constants, the frequency of appearance per unit time per unit area was measured and normalized to the cytoplasmic fluorescence intensity (in arbitrary unit) reflecting the relative concentration of SOS molecules in the cytoplasm. Residual TMR ligands in cells were negligible (Fig. 2.9). The relative association rate constants were similar among WT, REM(–) and AI(–) molecules before and at 3 and 8 min of EGF stimulation (Fig. 2.18B). The rate constants slightly increased from before to after EGF stimulation for 3 min, but this increase was not statistically significant, and nearly returned to basal level at 8 min. Considering the association and dissociation kinetics, we concluded that the REM(–) and AI(–) mutations altered the dynamics of SOS translocation by predominantly affecting the kinetics of dissociation from the plasma membrane.

### 2.3.3. Kinetic model of SOS dissociation from the membrane

A minima model of SOS dissociation kinetics was constructed (Fig. 2.19A), based on the finding that the G and H domains were solely responsible for extending

the dwell time of SOS (Fig. 2.12 and Material method). This model contained three association states for SOS (G, H and I) on the plasma membrane. G or H indicates the association state in which only the G or H domain interacts with the membrane, respectively. I is an intermediate state of dissociation, the formation of which requires both the G and H domains. In the I state, it is possible that the G and H domains associate with the membrane simultaneously, and any other membrane-binding domains and possible interactions between SOS molecules will affect the dwell times during this state. $\phi$ is the dissociation state in the cytoplasm. In this model, I assumed the dissociation rate constants of G and H domains ($k_{1r}$ and $k_{2r}$, respectively) are independent (i.e., $k_{1r}$ and $k_{2r}$ were common for the dissociations from the I state and from the H and G states). We also presumed that the total number of SOS molecules in cells remains constant. Although this is a coarse-grained model in that various possible structural states of SOS on the plasma membrane were degenerated into three kinetic states, it is the most basic model that can interpret the experimental dwell time distributions (Fig. 2.13C), and it provides a simple and unified explanation for the kinetic behaviors of WT and mutant SOS molecules.

We determined the dissociation rate constants for the G ($k_{1r}$) and H domains ($k_{2r}$) from the dwell time distributions of SOS fragments that contain the G domain or H domain alone (Fig. 2.10). Both distributions fit a single-component exponential function well, as assumed in the dissociation model. The estimated dissociation rate constant of the G and H domains were $k_{1r} = 1.5\ s^{-1}$ and $k_{2r} = 1.9\ s^{-1}$, respectively, after correction with the photobleaching rate constant ($0.05\ s^{-1}$; Fig. 2.11). These values did not change in cells that were stimulated with EGF (Fig. 2.11CD).

Dissociation of the G domain from plasma membrane possibly occurs through two pathways, i.e., dissociations of Grb2 from EGFR, and the G domain from Grb2. Single exponential kinetics suggest that one of these two pathways was the rate limiting, though I could not distinguish which one of them was the rate limiting pathway. Another possibility is that the two pathways have similar rate constants. To determine the initial conditions of the model, the relative association rate constants were measured for the G and H fragments (Fig. 2.14). Before and after (3 and 8 min) SOS activation, the sum of their rate constants approximated to that of WT. REM(–) and AI(–) displayed association rate constants that were similar to those of WT (Fig. 2.18B). Therefore, I assumed that in the initial association state of SOS [WT, REM(–), and AI(–)] and at every stage of cell stimulation, either the G or H domain interacts with the membrane independently at a fractional ratio that is proportional to the association rate constants of the G and H fragments. I estimated that, in the initial association states, the G:H is 0.7:0.3 (before EGF stimulation), 0.8:0.2 (at 3 min) and 0.7:0.3 (at 8 min).

### 2.3.4. Dissociation kinetics of SOS from the plasma membrane

The dwell time distribution of WT, REM(–) and AI(–) in single cells before and after EGF stimulation for 3 and 8 min (Fig. 2.12ADH) were fit with the dissociation kinetics model (Fig. 2.19A) using floating values of $k_1$ and $k_2$. As the result, the probability density distributions of the G, H and I state were estimated over time after the initial association of the molecule with the plasma membrane (Fig. 2.19B-D). The fraction of WT SOS molecules that dissociated via the intermediate (I) state increased after EGF stimulation and was sustained for at least 8 min (Fig. 2.19B).

For the REM(–) molecules, the I state fraction was enhanced at 3 min but returned to the basal level at 8 min (Fig. 2.19C). For the AI(–) molecules, the increase in the I state fraction was small (Fig. 2.19D). The fraction of I state during total dwell times was calculated from the time courses in single cells (Fig. 2.20A). The fraction of I state of REM(–) was smaller and less maintained than that of WT, suggesting that the interaction between REM domain and RAS-GTP takes place during the I state and stabilized the I state. The small fraction of the I state for AI(–) suggests that normal orientation between HL and H domain in the WT molecule, which is lost in AI(–), promotes the formation of the I state.

The results of the kinetics analysis suggest that the interaction between REM domain and RAS regulates the I state fraction but is not required for the I state formation. In addition, the fraction of SOS molecules in the I state corresponds to the membrane density of SOS, correlating with the extension of dwell times. The link between the I state faction and WT SOS density was examined in single cells after stimulation for 3 and 8 min (Fig. 2.20BC). I noted a positive correlation at both 3 min and 8 min, with a larger correlation coefficient at 8 min (0.84) than at 3 min (0.61), suggesting that at the later times, the SOS density on the plasma membrane depends more on the increase in I state, whereas in the early stage, there are mechanisms that increase the dwell time of SOS other than by increasing the I state. An increase of G state, which has a smaller dissociation rate constant than the H state, at the initial association (Fig. 2.14) must be one of these other mechanisms. It is possible that such I state independent mechanisms caused the extension in the dwell time of REM(–) at 3 min (Fig. 2.12D).

### 2.3.5. Measurement of RAS activation in living cells

To determine how the positive feedback reaction affects downstream reaction, I measured translocation of SOS and RAF to the plasma membrane in the same cells using dual-color single-molecule imaging (Fig. 2.21A). RAF is one of effector protein of RAS and recruited from the cytoplasm to the plasma membrane upon RAS activation [Leevers *et al.*, 1994; Stokoe *et al.*, 1994]. I transfected cells simultaneously with Halo7-SOS and GFP-RAS constructs, and monitored the EGF-induced translocation of TMR-SOS and GFP-RAF. Although the correlation was not clear at 3 min, the RAF density tended to be greater in cells with higher SOS densities. After cell stimulation for 8 min, there was a positive correlation between SOS and RAF densities on the plasma membrane (Fig. 2.21BC). Thus, the sustained translocation of SOS to the plasma membrane maintained RAS activation for RAF translocation. I noted an evident correlation between the fraction of I state and the density of SOS after stimulation for 8 min (Fig. 2.20C). Taken together, the fraction of I state, and thus the strength of the positive feedback loop between SOS and RAS, is related to the level of RAS activation at 8 min.

The function of the intact positive feedback reaction in RAS activation was noted when I measured the density of RAF on the plasma membrane of cells that expressed excess amounts of REM(–) or AI(–) molecules (Fig. 2.22). In these cells, the increased in RAF translocation after EGF stimulation was nearly abolished. Thus, in living cells, the association of RAS-GTP with the REM domain is required to induce an effective exchange of the nucleotide that is bound to RAS on the Cdc25 domain of SOS (i.e., the positive feedback between SOS and RAS is essential for

RAS activation). The normal orientation between the H domain and HL in SOS is another requirement for SOS function.

### 2.3.6. Discussion

In this study, I measured the dynamics and kinetics of WT, REM(–), and AI(–) molecules on the plasma membrane of living HeLa stimulated with EGF. Based on kinetic analysis of dwell times of the SOS molecules on the membrane, I identified an intermediate (I) dissociation state and formulated the function and dynamics of SOS in RAS activation, based on the fraction of the I state. Through this intermediate state, the positive feedback loop between SOS and RAS that was identified in biochemical *in vitro* experiments was shown to function in the context of living cells. The positive feedback is critical for RAS/RAF signal transduction in living cells.

The dwell time analysis of SOS on the plasma membrane suggests that both G and H domains are required for formation of the I state, which was detected based on the extension of the dwell time (Fig. 2.12ABF). Simultaneous associations of two domains bring a non-linearity in the I state formation, making the I state as a switch of SOS-mediated RAS activation. The interaction between SOS and RAS-GTP (feedback RAS) at REM domain stabilizes the I state, as shown from the extended dwell time of WT more than of REM(–). However, this interaction was not necessary for I state formation, because the I state also occurred with the REM(–) mutant (Fig. 2.20A). In the early stages (3 min) of EGF stimulation, an increase of the association rate constants of $k_1$ and $k_2$ resulted in the large I state fraction in WT and REM(–) molecules (Fig. 2.23). This increase must have been caused by the activation of EGFR that produces GRB2-binding site on the EGFR molecules and increases the

density of acidic phosphatidylinositol phosphates via the activation of PI3Ks. Stabilization of the I state by other membrane association domains of SOS, including REM, also results in the increase of $k_1$ and $k_2$ in this simple kinetic model. At 8 min, the fraction of I state was greater in WT than REM(–) (Fig. 2.20A), suggesting that WT SOS interacts with the feedback RAS during the I state. This interaction is not shown in the reaction scheme (Fig. 2.19A), but Figure 2.25 illustrates my model of SOS dynamics on the plasma membrane, including the interactions of SOS with RAS molecules. The accumulation of RAS-GTP on the plasma membrane after EGF stimulation might sustain the I state fraction in WT (Fig. 2.20A).

In the AI(–) mutant, the fraction of I state was modest at both 3 min and 8 min of cell stimulation (Fig. 2.20A). This mutation nearly completely inhibited RAF translocation and thus, the activation of RAS (Fig. 2.22B). These data suggested that the signal dependent conformation change is abnormal in AI(–). In the crystal structure, D140 and D169 interact with R552 to stabilize the association between the H domain and HL [Gureasko *et al.,* 2010] In the R552 mutant, which has been identified in Noonan syndrome patients [Roberts *et al.,* 2007], the interaction between H domain and HL will be lost, implicating R552G as a hyper-active mutant. In contrast, in the AI(–) (D140A) mutant, the interaction between D169 and R552 could be remained. Therefore, one explanation of my results is that in the AI(–), the autoinhibition conformation is maintained in G and H states, but the normal orientation between H and G domains is lost by D140A mutation, preventing the simultaneous association of these domains with the plasma membrane. Inhibition of the formation of I state in the AI(–) should cause its function to be lost in RAS activation, which requires the positive feedback loop between SOS and RAS. This

might be why D140A has not been identified in Noonan syndrome patients. This possibility must be examined in future studies.

The mechanism of positive feedback between SOS and RAS-GP is not precisely known. Since isolated Cdc25 domain of SOS targeted to the plasma membrane by tagging with a CAAX motif has been reported to be active [Quilliam *et a.l,* 1994], it is possible that the REM domain is inhibitory for the GEF activity in the Cdc25 domain and association of RAS-GTP with the REM domain releases this inhibition. Then, the role of I state formation is to change the SOS structure to allow the release of inhibition. Another possibility is that elongated membrane association of Cdc25-CAAX was sufficient for RAS activation. In this case, dwell time elongation by the concerted function of H, G and REM domains is crucial for WT SOS to activate RAS.

The sustained translocation of SOS in cells seems to require the positive feedback loop between SOS and RAS, because it is lost in REM(–) and AI(–) (Fig. 2.17C). But how the molecular kinetics sustains this translocation in ensemble molecules is unknown. If the positive feedback between SOS and RAS functions autonomously, it will induce continuous activation of RAS. However, in the steady-state dynamics, although the accumulation of RAS-GTP (feedback RAS) on the cell surface increases the proportion of active SOS in the I state as shown in my kinetic model (Fig. 2.24A), SOS activity will return to basal levels unless RAS-GTP also induces the SOS translocation to the membrane [Hall *et al.,* 2001]. Because the REM(–) mutant did not have a lower association rate with the membrane (Fig. 2.18B), it is improbable that RAS-GTP increases the SOS translocation under the conditions in living cells stimulated with EGF. I observed a slightly higher association rate

constant for WT SOS with the membrane after stimulation for 8 min versus before stimulation (Fig. 2.18B), but the difference was not statistically significant. Therefore, the sustained translocation of SOS might not be a quasi-steady state, but slow transient dynamics.

Regardless of the mechanism that sustains the SOS/RAS feedback, the positive feedback loop between SOS and RAS is not merely regulatory but is critical for RAS activation (Fig. 2.22A). This requirement for the positive feedback loop inevitably results in a nonlinear switch-like input-output relationship between SOS translocation and RAS activation. This response of the SOS/RAS system is advantageous in preventing spontaneous mis-activation and in amplification of small signals below critical levels. Yet, simultaneously, it might induce large cell-to-cell deviations with similar inputs when the small differences in the initial and/or boundary conditions are amplified. It is likely that the wide cell-to-cell variability in the sustained translocation of WT SOS (Fig. 2.17C) is caused by the positive feedback loop. In contrast, negative feedback from ERK, which is activated downstream of RAF and phosphorylates the G domain of SOS to prevent interaction with GRB2 [Corbalan-Garciaet *et al.*, 1996], is a mechanism that might impede SOS translocation at the later stage (> 8 min) of cell stimulation.

In conclusion, this study indicates that an intermediate state formation functions as a switch of SOS activity, corresponding to the establishment of the positive feedback loop between SOS and RAS. The multiple membrane-associating domains of SOS, particularly the H, REM and G domains function in concert during the intermediate state of membrane association, in which SOS interacts with the feedback RAS molecule to be a fully active GEF for RAS. Because the RAS

activation requires the positive feedback domain of SOS, the SOS/RAS positive feedback is crucial in regulating the diverse functions of growth factors that lie upstream of SOS. Various point mutations in SOS induce RAS-RAF syndromes [Lepri *et al.,* 2011]. Some of these mutations have been detected in SOS domains which do not directly control nucleotide exchange on RAS, and their pathological mechanisms are unclear. My study raises the possibility that these mutations affect SOS function by altering the coordination among multiple SOS domains.

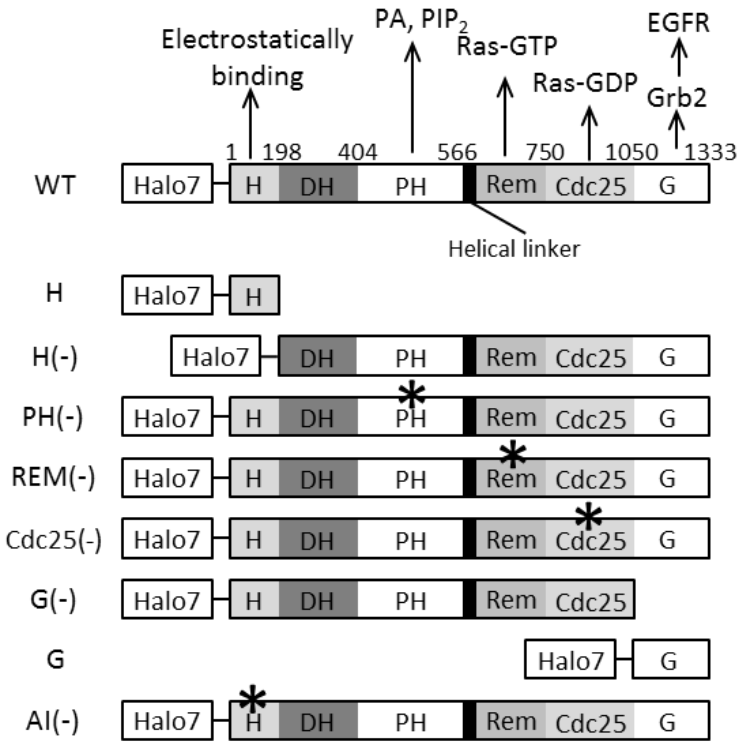


**Figure 2.1. Domain structure of SOS structure**

Halo7 tagged SOS WT and mutants were expressed in Hela cells. Halo7 tag is located at N-terminus of SOS. WT structure shows membrane components which interact with each domain. H, H(-), G(-) and G are deletion mutants Δ198-1333, Δ1−191, Δ1066−1333 and Δ1−1049, respectively. Other mutants are point mutants which lack the membrane associating function. Mutation site is shown by an asterisk. PH(-) is a quadruple mutant, K456E/R459E/H475E/R479E. REM(-) is a triple mutant, L687E/R688A/W729E. Cdc25(-) and AI(-) are single mutants, F929A and D140A, respectively.

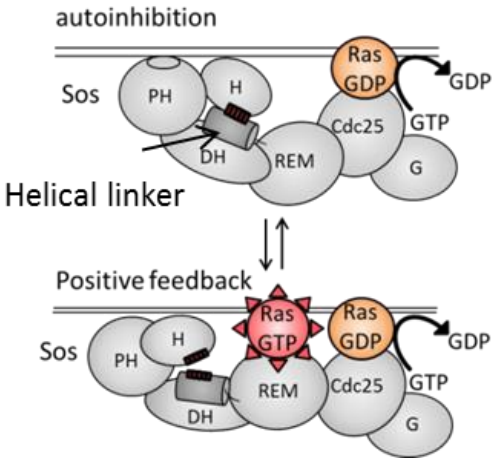


**Figure 2.2. Diagram of SOS/RAS positive feedback**

Interaction between REM domain of SOS and RAS-GTP promotes nucleotide exchange of RAS. This positive feedback is inhibited by autoinhibited conformation of SOS in resting cells. In autoinhibition state, DH domain disturbs the interaction between the REM domain and RAS-GTP. The interaction between H domain and helical linker (HL) stabilizes autoinhibition state. When the interaction between H domain and HL is released, REM domain can interact with RAS-GTP.

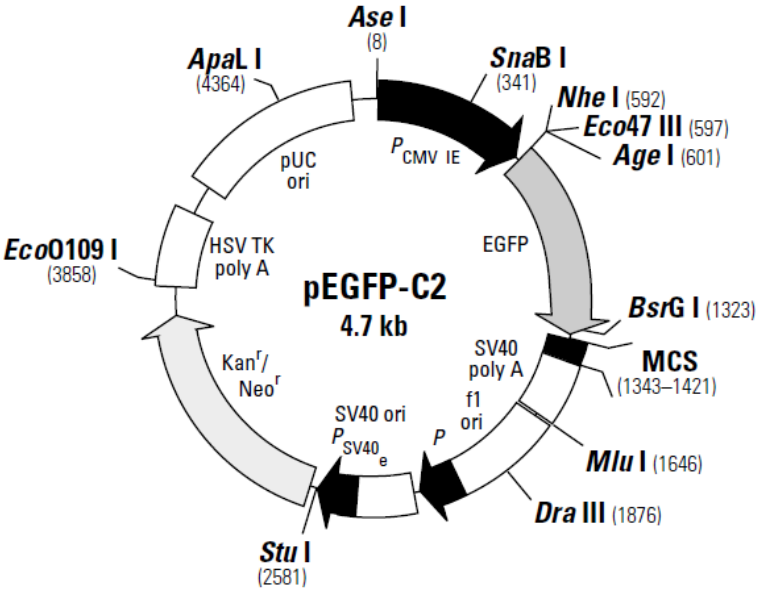


**Figure 2.3. Circle map of pEGFP-C2 vector**

The hSOS1 was inserted into pEGFP-C2 vector. This map was abstracted from BD Biosciences Clontech Vector information

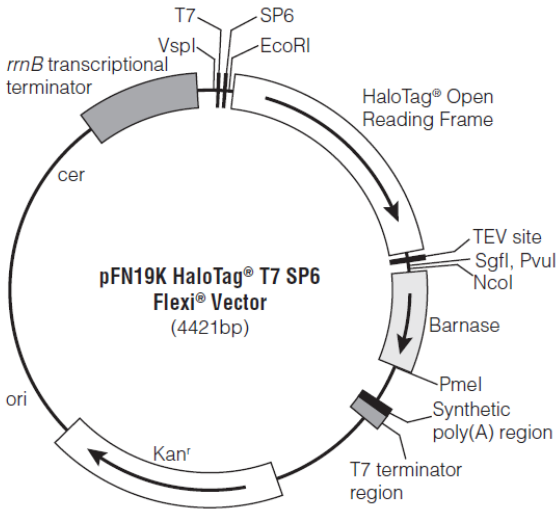


**Figure 2.4. Circle map of FN19K HaloTag T7 SP6 Flexi Vector**

Halo tag was cloned into FN19K HaloTag T7 SP6 Flexi Vector. This vector was bought from Promega.

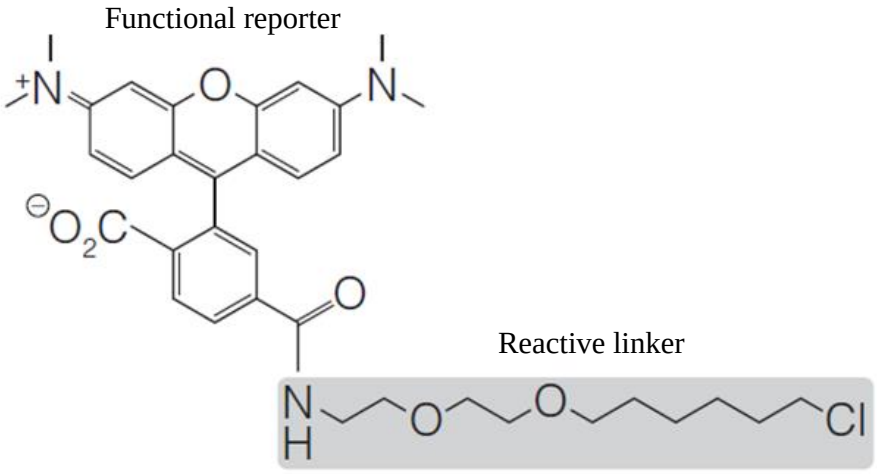


**Figure 2.5. Structure of TMR**

Structure of Halo tag TMR ligand is shown. TMR consists of functional and reactive linker. MW is 636 g/mol. There is a pocket at catalytic site in Halo7 protein. The reactive linker is inserted into this pocket, forming covalent binding.

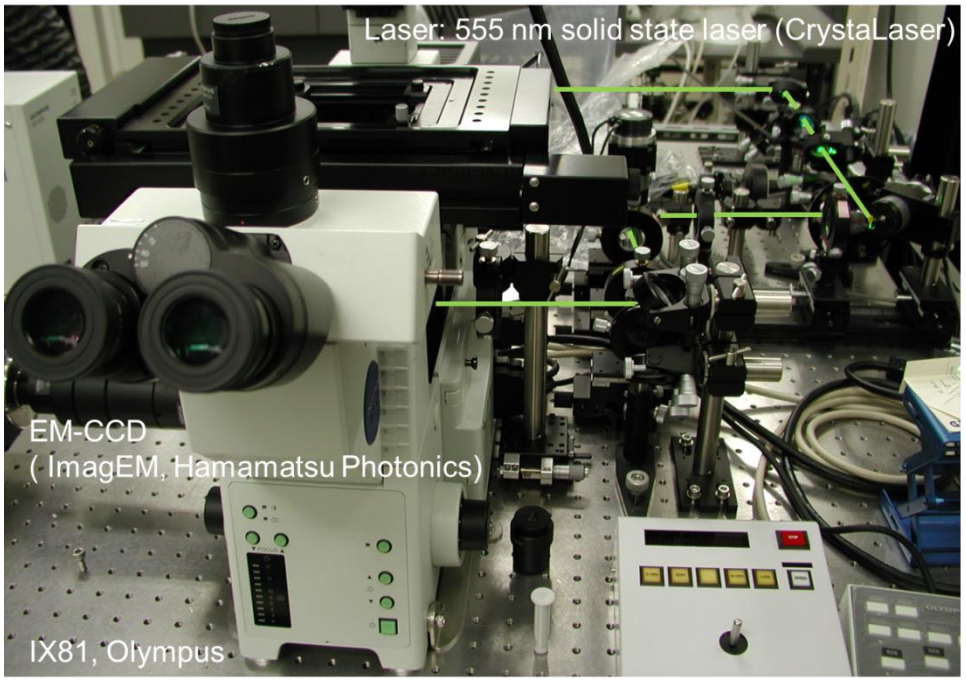


**Figure 2.6. Setting of TIRM (IX83, Olympus)**

Halo-SOS was illuminated with a 555nm solid laser. Fluorescence signal was detected by using EM-CCD.

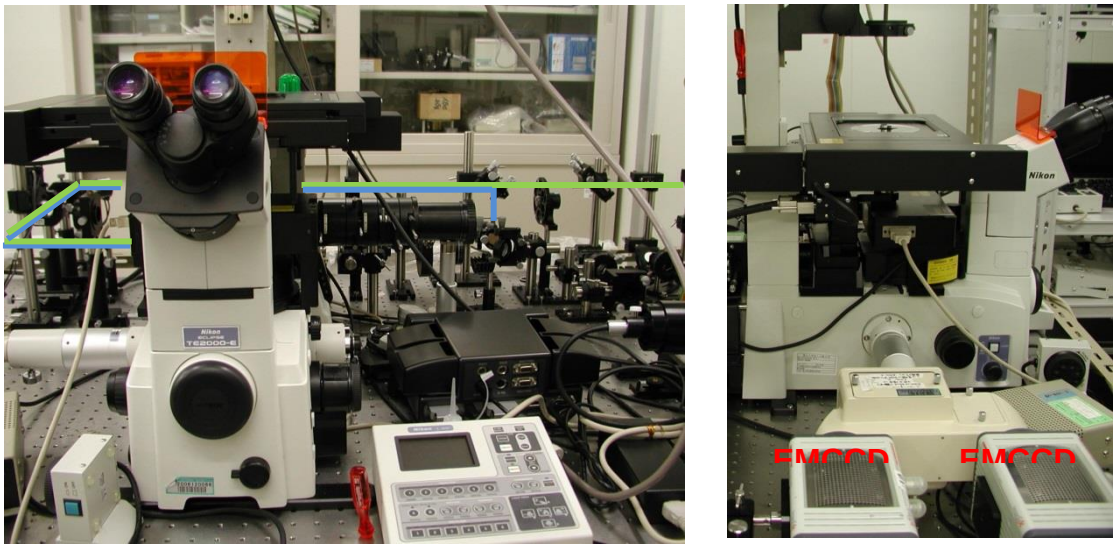


**Figure 2.7. Setting of W view system**

Halo7-SOS and GFP-RAF were illuminated with a 559 nm and 488 nm solid laser. The illumination was divided by the dichroic mirror (493/574).

Fluorescence signals were divided by emission filter (FFF640-FDi01) and detected by EMCCD respectively.

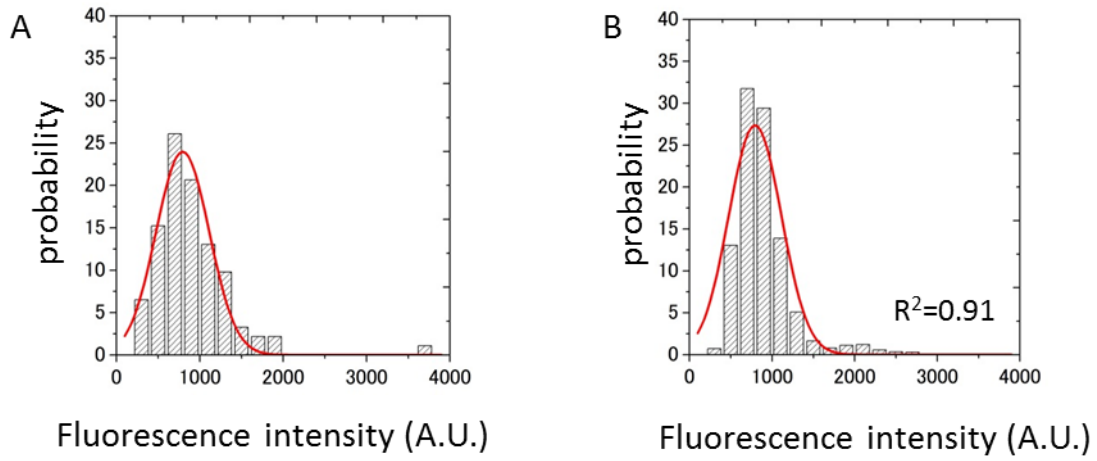


**Figure 2.8. Intensity distribution of TMR-SOS in fixed and living cells**

A) Distribution of photobleaching step size for single TMR-SOS molecules on the membrane in fixed cell. This distribution shows that the intensities of each single particle averaged for 2 video frames immediately prior to photobleaching. Red line indicates the Gaussian function fitted to the histogram. B) Fluorescence intensity distribution of TMR-SOS particles on the membrane in living cells before stimulation is shown.

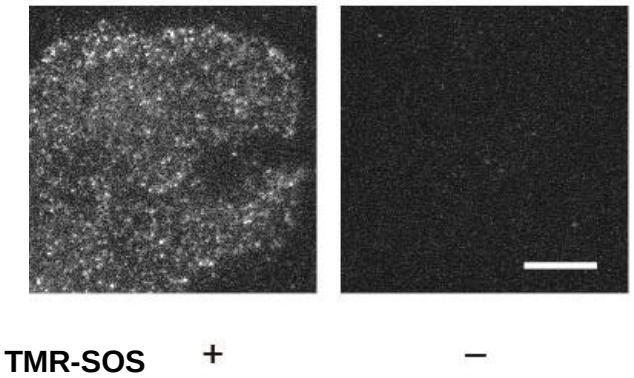


**Figure 2.9. Single molecule imaging of TMR-SOS on cells**

The images were acquired on the membrane in cells with (+) or without (-) transfection by using TIRFM. Slight numbers of fluorescent spots were detected in cells without transfection, indicating Halo-specific TMR labeling. Scale bar shows 10 μm.

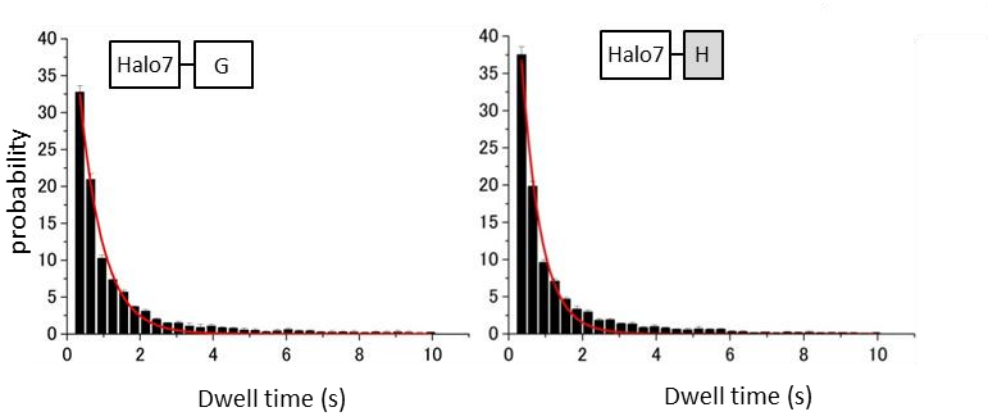


**Figure 2.10. The dwell time distributions of G domain and H domain**

The distributions before EGF stimulation (bars) were fitted with a single exponential function (red lines). The estimated dissociation rate constants were $k_{1r}$=1.5 $s^{-1}$ and $k_{2r}$=1.9 $s^{-1}$. Similar results were estimated when the distributions were fitted after cell stimulation for 3 and 8 min (Fig. 2.11CD).

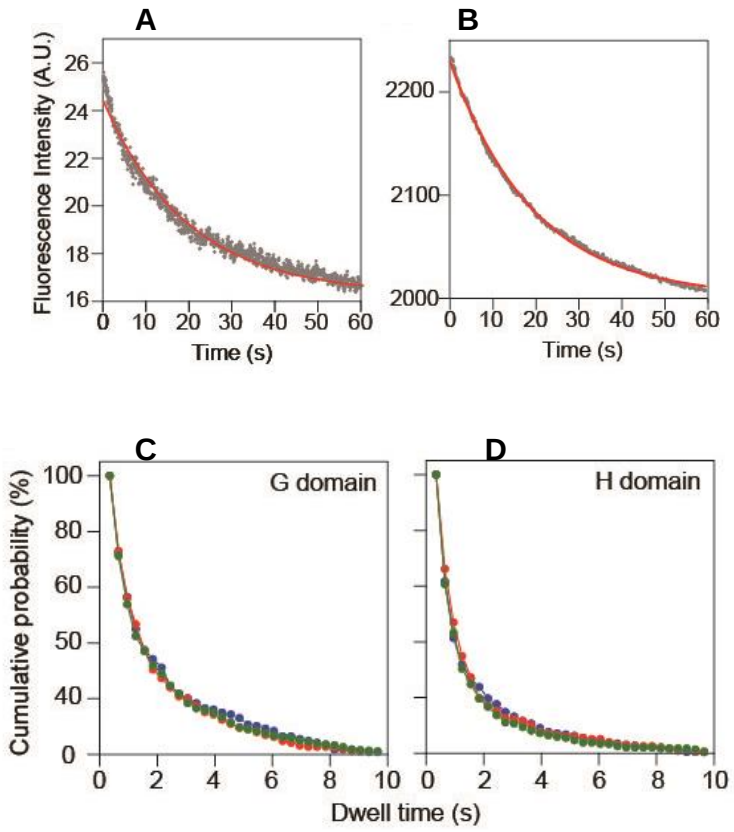


**Figure 2.11. The dwell time distribution and photobleaching time course**

A) Photobleaching time course of TMR-SOS (gray) on the membrane of the fixed cell. The time course was fitted with single exponential function (red line). The estimated photobleaching time constant is 19.6 s. B) Photobleaching time course of TMR-EGFR (gray) on the membrane of the living cell. cDNA of human EGF receptor (pNeoSRαII) was cloned into the HaloTag vector using PCR to construct EGFR-Halo. Cells transfected with cDNA of EGFR-Halo were stained with Halo-Tag ligand and measured using a TIRFM under the same conditions as in the imaging of TMR-SOS. C,D) Cumulative dwell time distribution of the G (left) and H domains (right) before (blue) and after EGF stimulation for 3 (red) and 8 min (green).

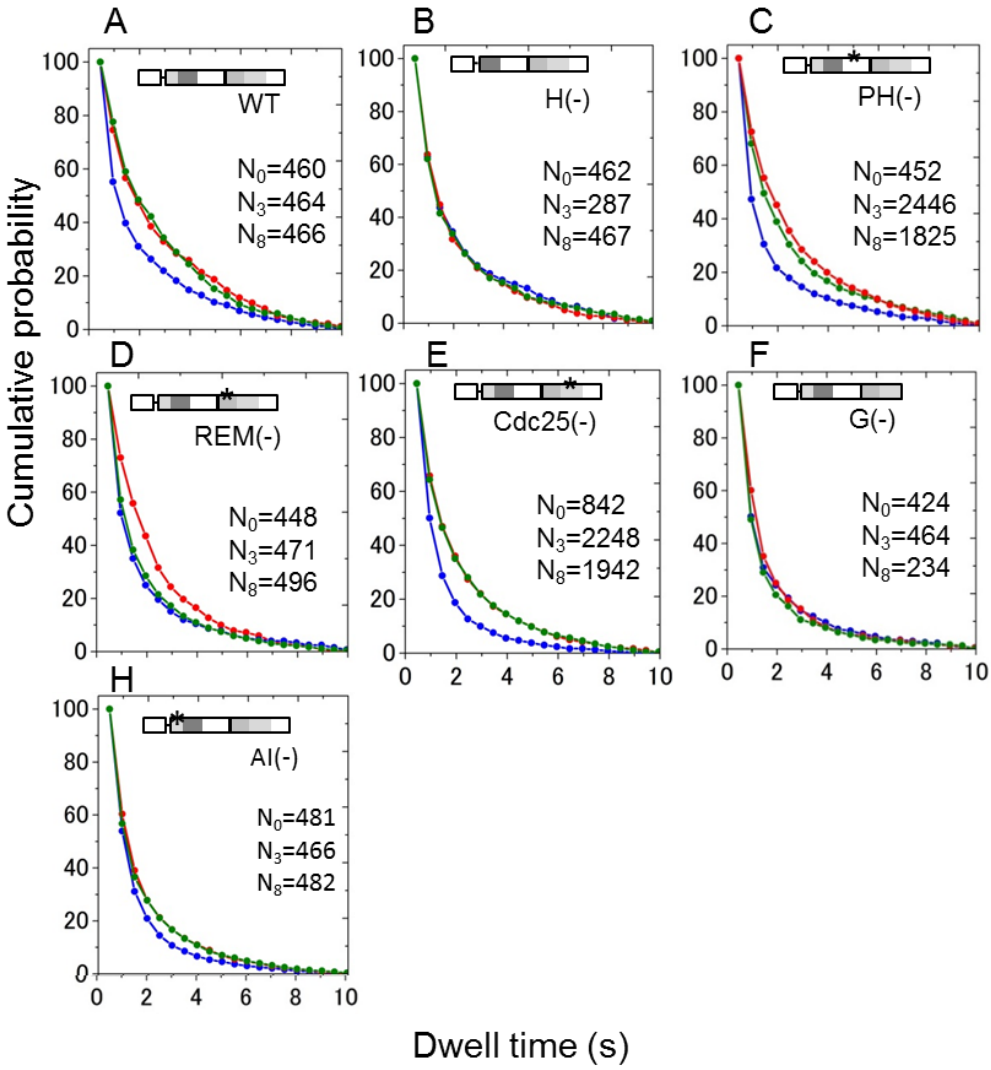


**Figure 2.12. Dwell time distributions of WT and mutants**

Typical cumulative distribution of dwell time for the same single cells before (blue) and after EGF stimulation for 3 (red) and 8 min (green) is shown. The distributions at 3 min (red line) for AI(-) and Cdc25(-) nearly overlap with the distribution at 8min (green lines). $N_0$, $N_3$ and $N_8$ show the numbers of fluorescent spots before and after stimulation for 3 and 8 min respectively. These distributions were normalized.

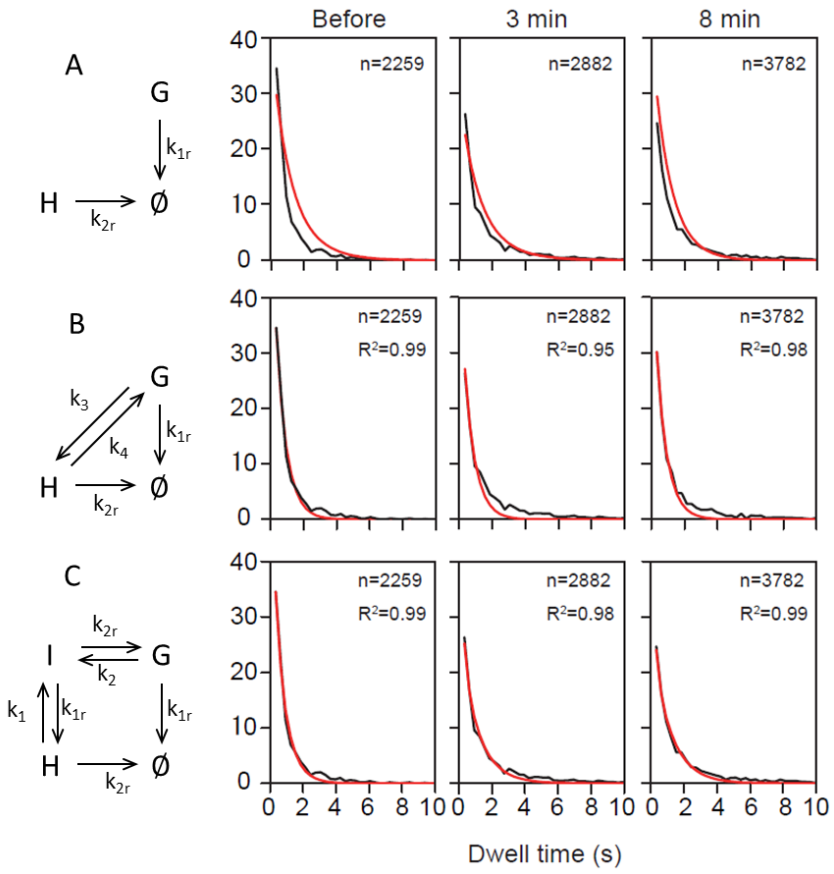


**Figure. 2.13. The dissociation kinetic models and fitting results**

The dwell time distributions of WT before and after EGF stimulation for 3 and 8 min were fitted with different kinetic models. A) Sum of two independent exponential components. B) Direct transitions between the H and G states. C) Involvement of an intermediate (I) state. Black line shows dwell time distribution measured by the experiment. Red line indicates fitting result. The fitting results of model A and model B were systematic differences from the experimental data. n means number of particles analyzed. $R^2$ means coefficient of determination. $\chi^2$ shows chi square between the data and fit functions.

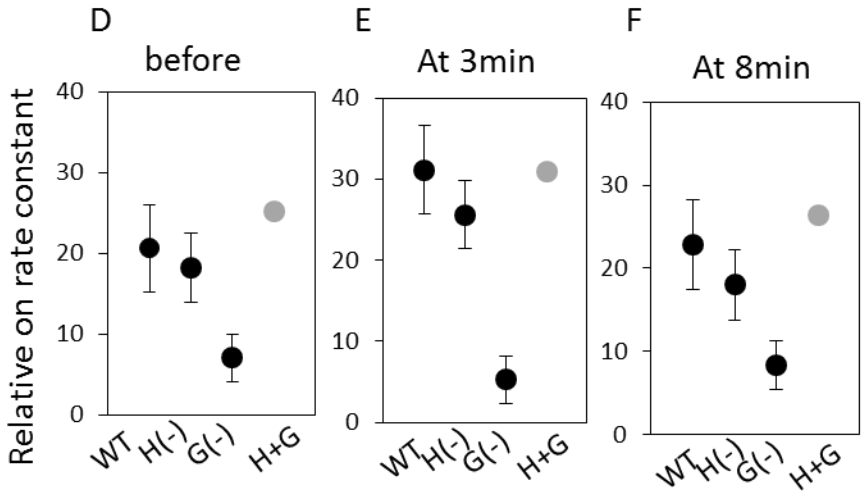


**Figure 2.14. The relative association rate constants before and after stimulation for 3 min and 8 min**

In all periods, WT was calculated by the sum of H (-) and G (-). Similar data was taken in G and H mutants. Black dot shows experimental data. Gray dot indicates the sum of average value in H (-) and G (-). Error bar means S.E.

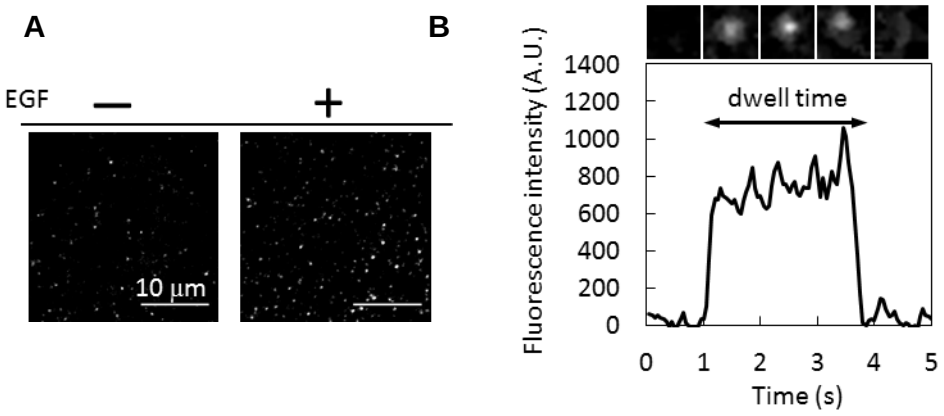


**Figure 2.15. The images of SOS molecules on the membrane and the time course of single molecule intensity**

A) Snapshot from single-molecule movies of TMR-SOS by using TIRFM. The images were taken on the plasma in living cells membrane before and at 3min after EGF stimulation. The number of SOS increased at 3 min after stimulation. B) A typical time course of single molecule on the membrane is shown. The period between the appearance and disappearance of molecules was measured as the dwell time on the plasma membrane.

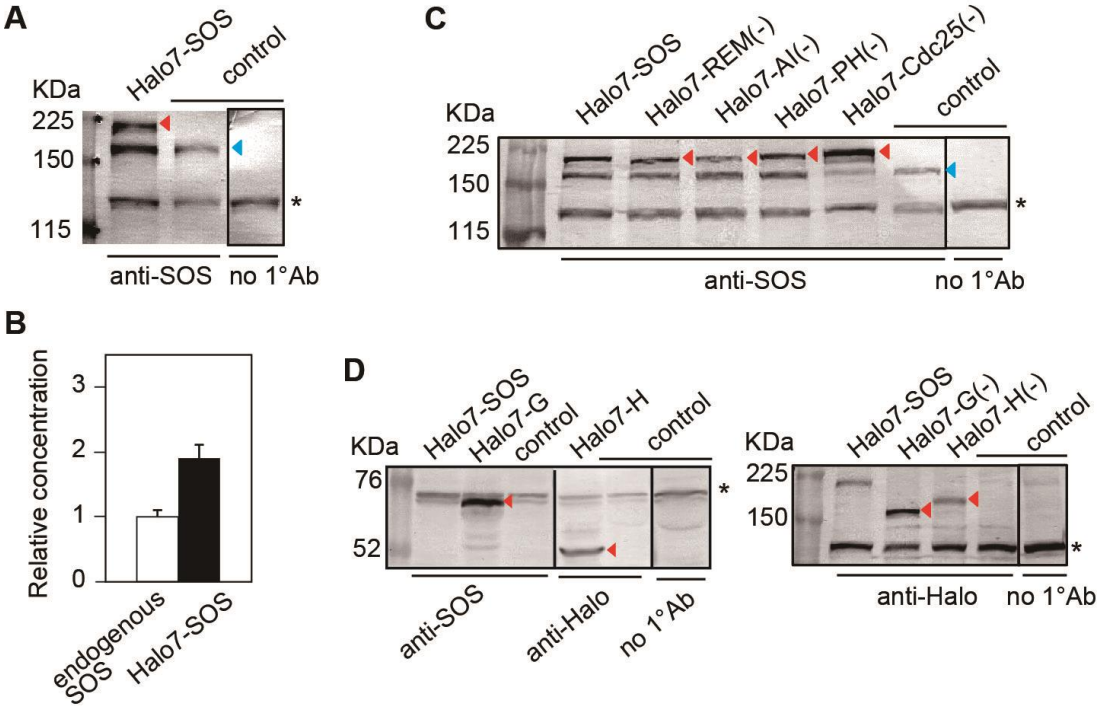


**Figure 2.16. Immunoblotting analysis of SOS**

A) Expression of Halo7-SOS and endogenous SOS was detected with anti-SOS. The expected molecular weights of Halo7-SOS and SOS were 187 and 152 kDa. B) Expression of Halo7-SOS relative to that of endogenous SOS was quantified from the staining intensities in the immunoblotting analysis. Error bar means S.E. C) Expression of point mutants of SOS was detected with anti-SOS. D) Expression of deletion mutants of SOS was examined with anti-SOS and anti-Halo-tag. The expected molecular weights of Halo7-tagged G, H, G(-) and H(-) were 64, 57, 159, 165kDa, respectively. Red triangles mean SOS molecules expressed after transfection. Blue triangles show endogenous SOS molecules. Stained areas which derive from non-specific association of the secondary antibody were marked with asterisks.

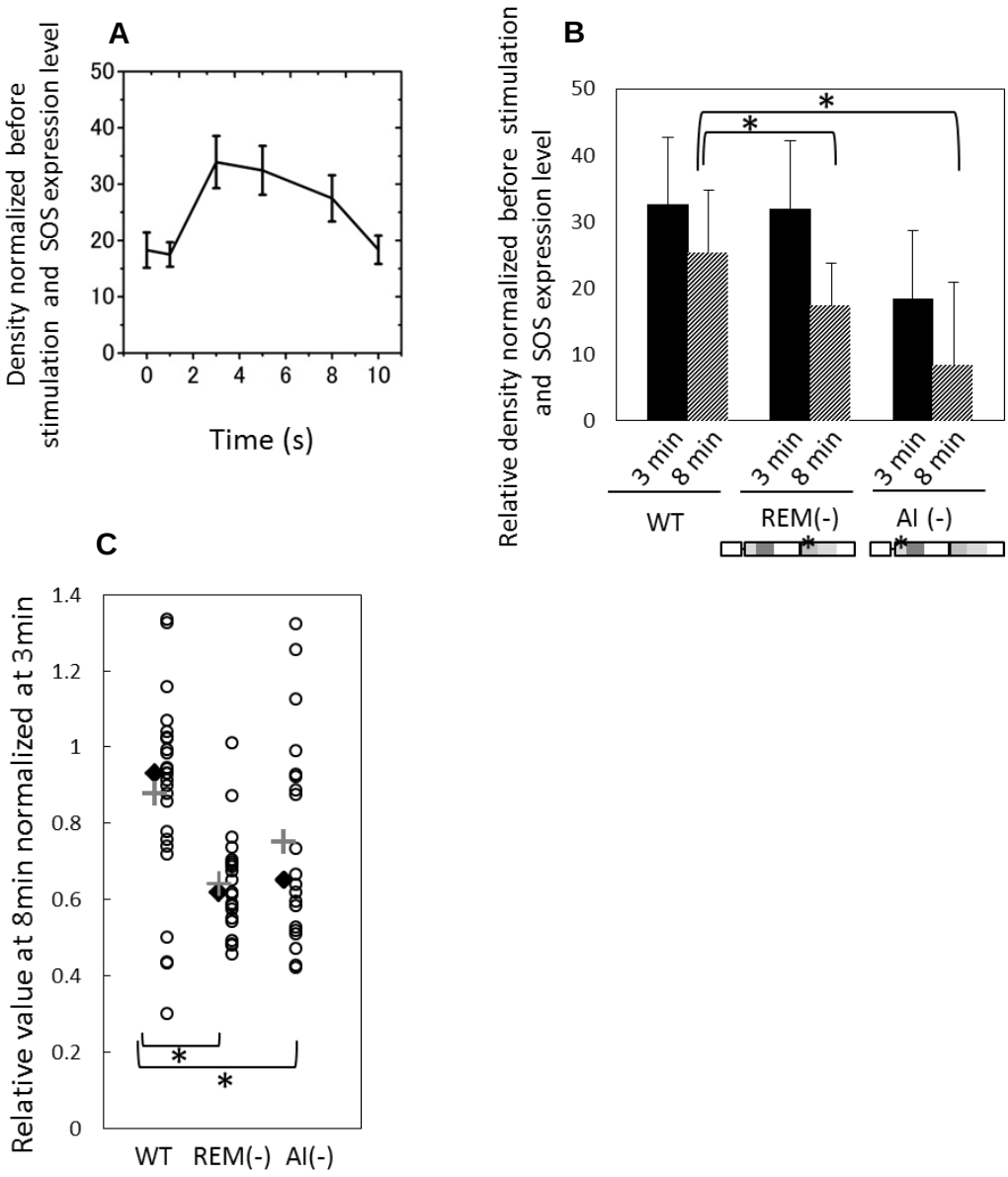


**Figure 2.17. Time course of the SOS molecule density**

Ensemble-molecule time course of the WT SOS translocation on the membrane was shown. At time 0, the cells were stimulated with EGF. The density of SOS molecules was normalized to SOS expression levels. The mean values for 10 cells were shown with S.E. B) SOS density were measured in single cells after EGF stimulation for 3 min and 8 min, normalized to SOS expression levels and averaged over 25, 21 and 20 cells expressing WT, REM(-) and AI(-), respectively. Error bar means S.E.

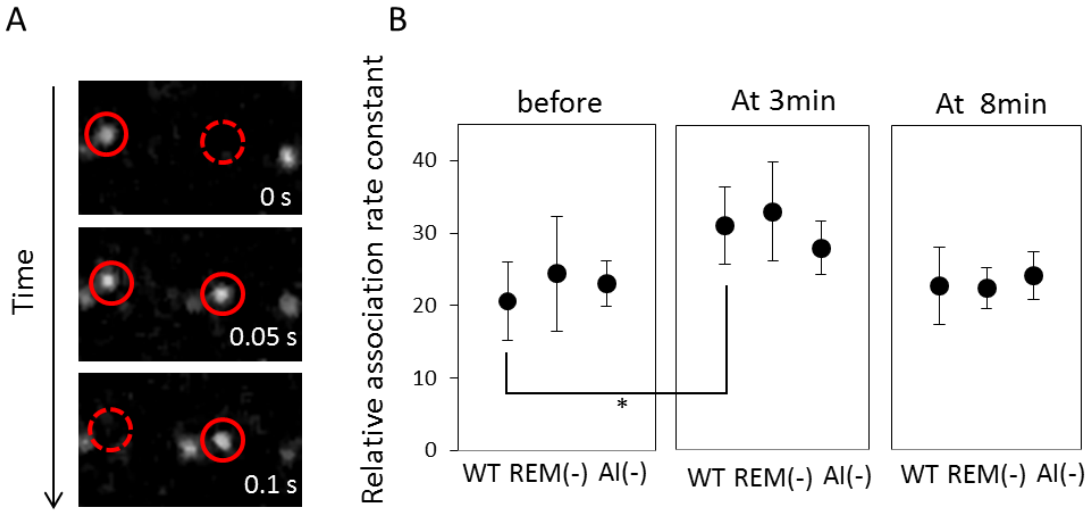


**Figure 2.18. Relative association rate constant**

A) Appearance and disappearance of molecules were measured using TIRFM. B) The frequency of appearance (number of TMR-SOS molecules per unit time) in the unit area were normalized to SOS expression levels, which is the relative association rate constant. SOS expression levels mean fluorescence intensity of TMR-SOS in the cytoplasm measured in arbitrary units. The mean values of the frequencies in WT, REM (-) and AI (-) were measured in 11, 10 and 11 cells, respectively. Error bar shows S.E.

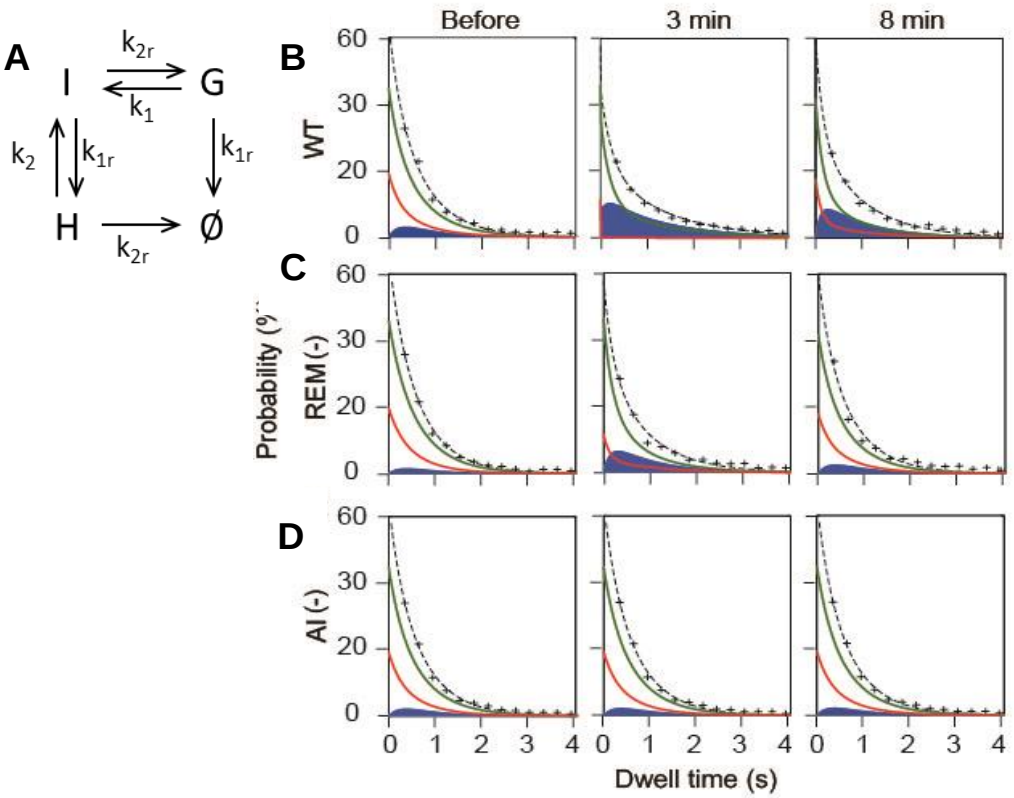


**Figure 2.19. Dissociation kinetics model and fitting results**

A) The dissociation kinetic model of SOS from the plasma membrane is shown. SOS has three association states. In G and H state, either G domain or H domain associates with the plasma membrane. In I state, G domain and H domain binds to the membrane simultaneously. B-C) Typical dwell-time distributions (plus symbols) were fitted by this kinetic model. Black dotted line, red lines and green lines show the result of fitting for the total, H and G states. Blue areas indicate the total fractions of the I state.

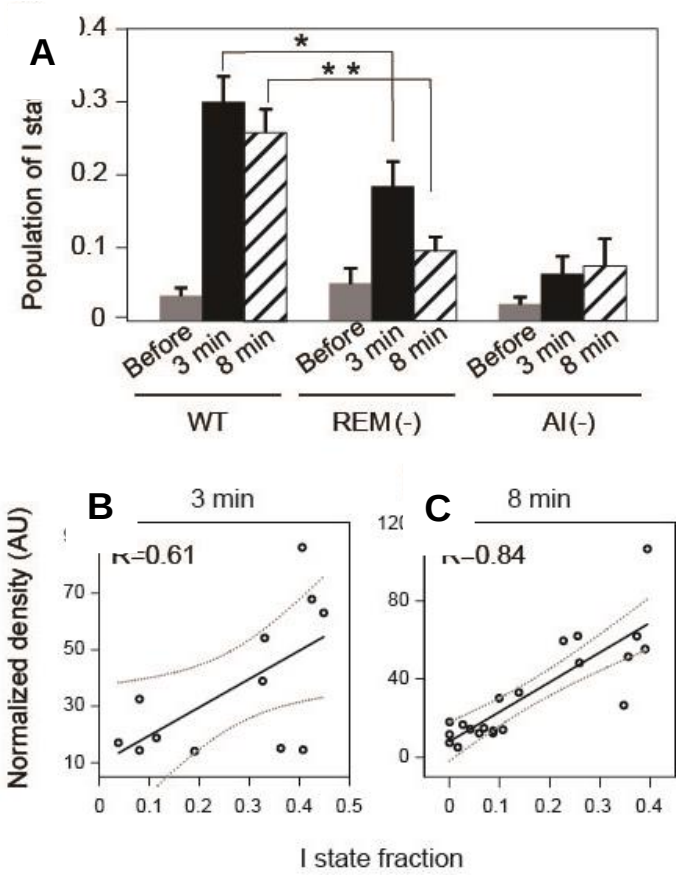


**Figure 2.20. The time course of the I state fraction and the correlation between SOS density and I state fraction**

A) The fraction of I state before and after EGF stimulation for 3 and 8 min were described. The mean values for 5 and 9 cells expressing WT SOS (before and after stimulation respectively), 5, 9 and 7 cells expressing REM(-) (before, 3 min and 8 min, respectively) and 6 and 5 cells expressing AI(-) (before and after stimulation, respectively) are shown. * and ** means $p<0.05$ and $p<0.001$, on Mann-Whitney test. B,C) The normalized densities of WT on the membrane was plotted against the I state fraction in the dissociation kinetics. The densities were normalized to SOS expression levels. The plots at 3 min (B) and at 8 min (C) after EGF stimulation were shown. Open dots represent values in single cells. Regression lines (solid line) are shown with their 95 % confidence intervals (dotted line). R means the correlation coefficient.

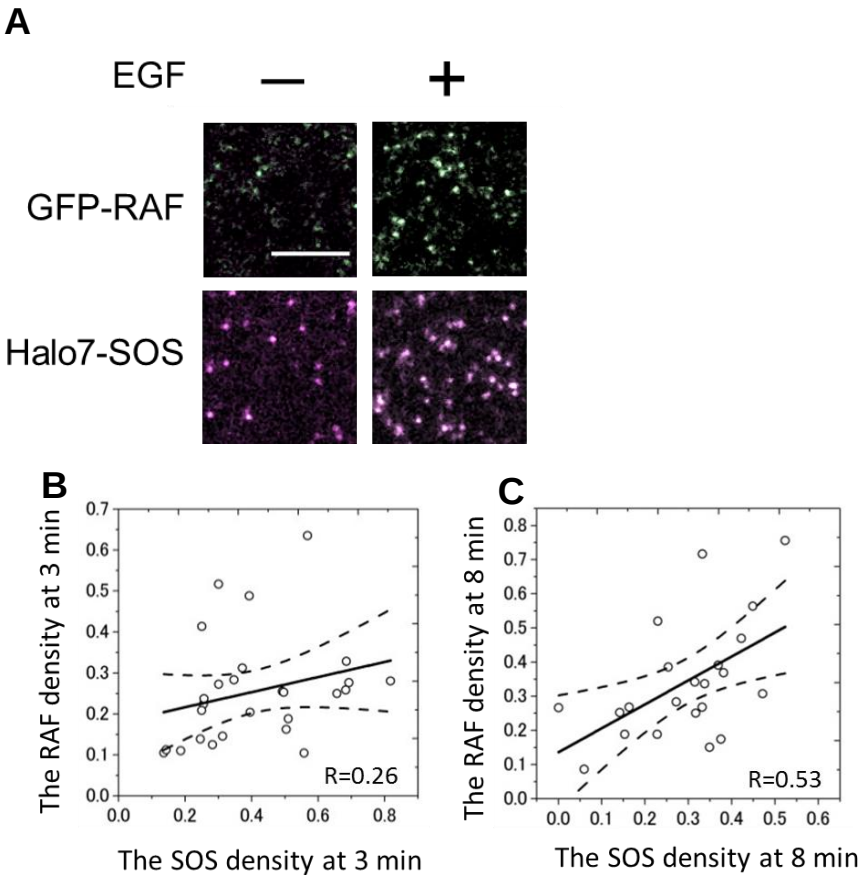


**Figure 2.21. Single molecule images of SOS and RAF, and the correlation**

A) Before (-) and at 3 min (+) after EGF stimulation, dual color of single molecule images of WT TMR-SOS and GFP-RAF on the membrane in the same cell were taken. Scale bar shows 10 μm. B,C) The densities of SOS and RAF were normalized to SOS and RAF expression levels, respectively. Open dot means the values in single cells. Regression lines (solid line) are shown with their 95 % confidence intervals (dotted line).

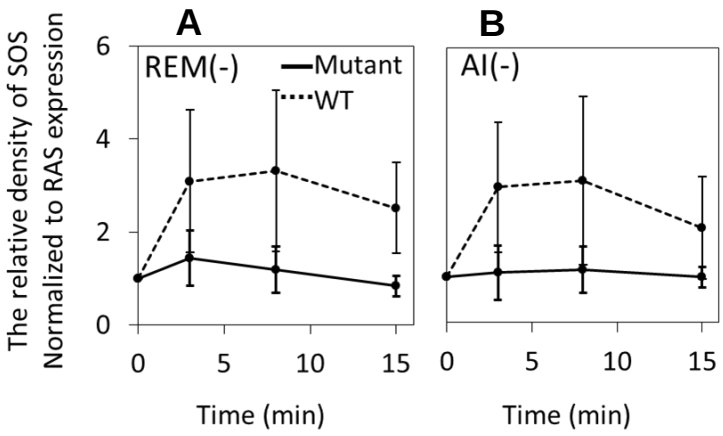


**Figure 2.22. The density of RAF in cell overexpressing WT SOS and mutants**
The time courses of RAS density on the membrane in cells expressing WTSOS or mutants excessively were shown. Excess amount of SOS mutants were expressed to examine the dominant negative effects on RAS activation. At 0 min, cells were stimulated. Dotted and solid lines indicate WT and the mutants, respectively. The mean values ± S.E. for 15, 5 and 5 cells expressing WT, REM(-) and AI(-), respectively, are shown.

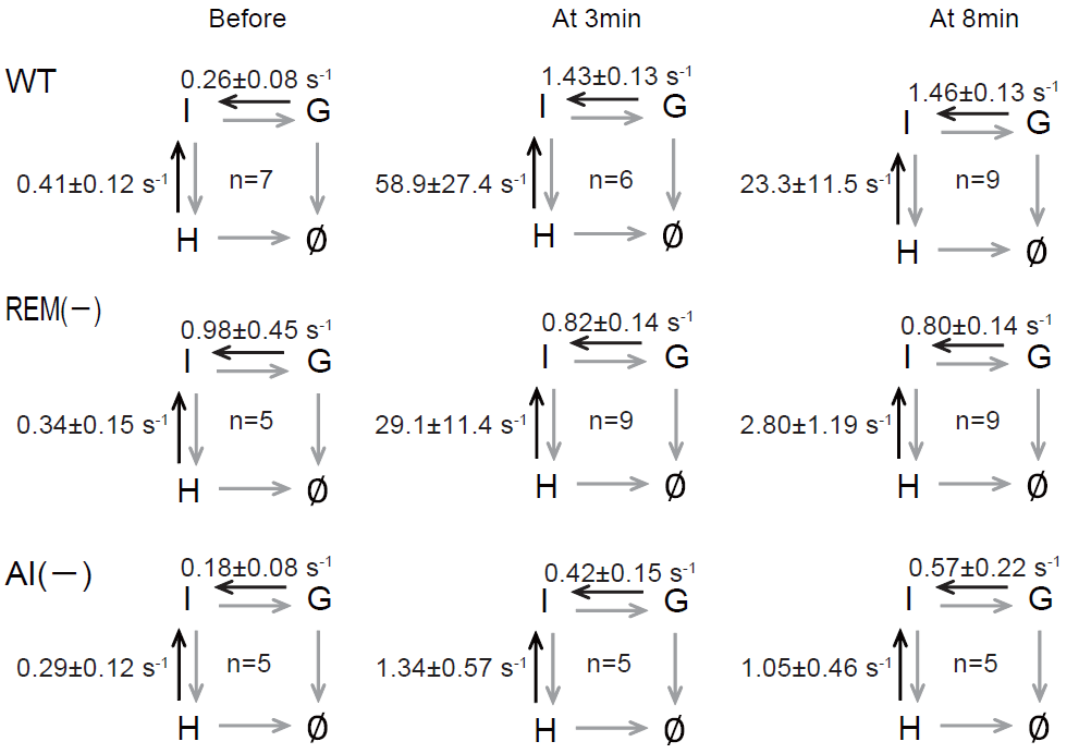


**Figure 2.23. The best-fit values of the association rate constants of WT and mutants**

The best-fit values for $k_1$ and $k_2$ were determined from the dwell time distributions. The mean values ±S.E. for n cells (n= number of cells) are described. The value of $k_1$ which is association rate constants of the G domain from the H state was significantly increased.

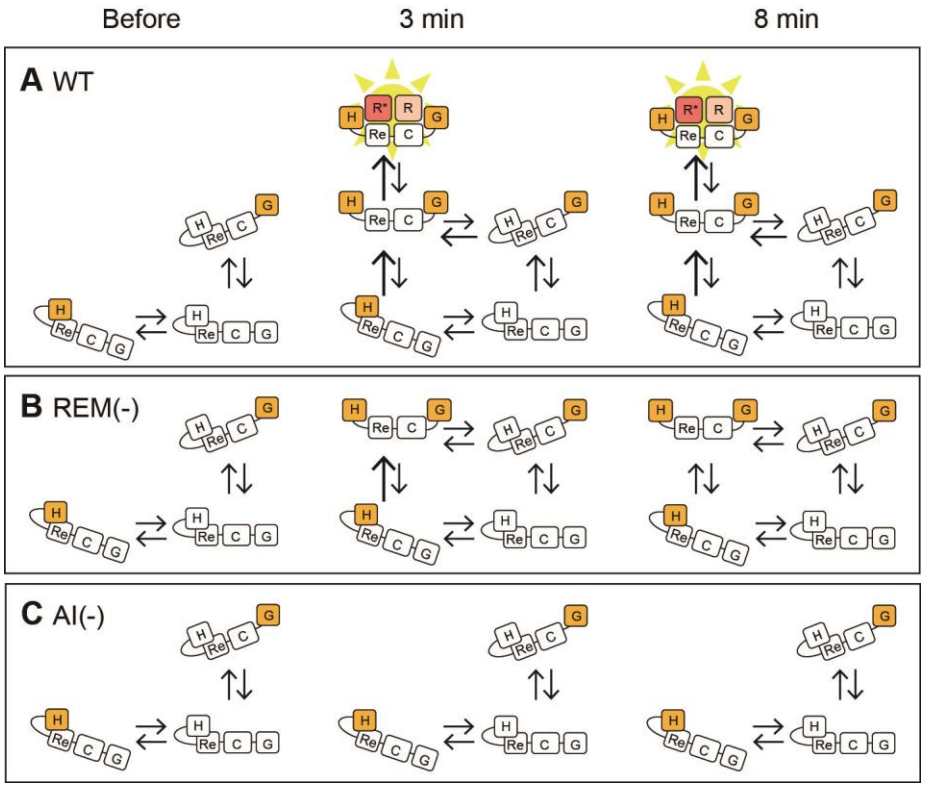


**Figure 2.24. The proposed models of SOS interactions with the membrane**

A) WT SOS in cytoplasm initially associates with the plasma membrane through either G or H state. With EGF stimulation, a conformational transition then takes place, changing into the dissociation intermediate (I state). The I state can be a mixture of multiple substates, in which other membrane-associating domains (PH, REM and Cdc25) of SOS are involved. During the I state, REM domain interacts with feedback RAS (RAS-GTP), and the GEF activity of SOS is stimulated. B) REM(-) SOS takes the I state, but because it does not interact with feedback RAS, its GEF activity is not stimulated. C) AI(-) SOS cannot assume the I state. Re, C, R and R* shows the REM domain, Cdc25 domain, RAS-GTP and RAS-GDP, respectively.

# Chapter III

## 3. Dissolution of coordinated SOS interactions by abnormal domain function derived from Noonan syndrome mutation

## 3.1. Introduction

Noonan syndrome (NS) is characterized by heart defect, short statue, and ectodermal abnormalities [Allason *et al.,* 1985; Mendez and Opitz 1985]. NS patients have single or multiple mutations in components of RAS-MAPK pathway such as KRAS and PTPN11. In addition to these proteins, the point mutation in Son of Sevenless (SOS) resulting in NS was found in 2007. And the mutation in SOS has been identified approximately 10-17% in patient of NS [Roberts *et al.,* 2007; Tartaglia *et al.,* 2007; Narumi *et al.,* 2008]. At present, NS patients are provided with only the symptomatic therapy because suitable treatment for each mutated protein is still unknown.

My study suggested that signal dependent RAS activation in living cells requires SOS/RAS positive feedback, and that this SOS/RAS positive feedback is regulated by interactions between membrane associating domains in SOS (Chapter II). The mutations in SOS identified in NS patients are located in various domains. And most of the mutations are located not in Cdc25 domain, which has catalytic site for RAS, but in other domains. Additionally, some of these mutations are known to cause excess activation of Ras-MAPK pathway like RAS activation and ERK phosphorylation [Roberts *et al.,* 2007; Chen *et al.,* 2010; Tartaglia *et al.,* 2007]. These reports suggest the possibility that abnormal interactions between SOS domains are one of the causes for excess RAS activation in living cells. But it is unclear whether mutated domains of SOS have abnormal function and induces the change of the SOS dynamics, resulting in RAS activation. And if so, whether the abnormal SOS dynamics is caused by the difference of molecular mechanism derived from each mutation, respectively.

In this chapter, I focused on NS mutants (R552G, M269R, R1131K) of SOS.

I observed these three mutants in living HeLa cells by single molecule imaging. And interaction kinetics of SOS molecules with the plasma membrane was analyzed in view of the regulation of SOS/RAS positive feedback that is crucial for RAS activation.

By alteration of interaction between RAS-GDP and the catalytic domain of SOS, the RAS activation could be modulated [Burns *et al.,* 2014; Leshchiner *et al.,* 2015]. My data suggest the possibility that RAS activation with EGF stimulation can be controlled by modulation of interaction between SOS domains or affinity of SOS domain for the membrane. I consider that this study leads to the appropriate treatment for NS according to mutations.

## 3.2. Material and methods

### 3.2.1. Preparation of plasmid and cell

Halo7 plasmid vector derived from the FN19K Halotag T7 SP6 Flexi Vector (Promega). And SOS point mutants were constructed into Halo7-SOS using the QuikChange Lighting Site-Directed Mutagenesis Kit (Agilent Technologies) PrimeSTAR® Max DNA Polymerase (Takara). Mutants used in this study are shown in Figure 3.1. All plasmids were expressed in HeLa cell. Cells expressing SOS were stained with 100 nM HaloTag® TMR Ligand (Promega). Construction of GFP-RAF plasmid was described in Hibino et al, 2003. Detail of plasmid construction and experimental condition is described in Chapter II.

### 3.2.2. Single-molecule imaging and analysis

The fluorescence images were acquired using CMOS camera (ORCA-Flash4.0, Hamamatsu Photonics) at the frame rate of $20s^{-1}$ based on an inverted microscope (IX83, Olympus). Acquired images were averaged in MetaMorph (molecular devices) and subtracted background in Image J (the National Institutes of Health). Single molecules detection and tracking were performed by home-made software and TrackMate [Jaqaman et al, 2008]. Dissociation kinetic analysis and statistics analysis were performed using Matlab (The Math Works) and Origin (Origin Lab). Detail of kinetic analysis is described in Chapter II.

## 3.3. Result and discussion

### 3.3.1. NS mutants had a common feature of increase in localization on the membrane

By using total internal reflection fluorescence microscope (TIRFM), Halo7 tagged SOS (Halo-SOS) conjugated TMR was observed in HeLa cells. This single molecule measurement system was described in Chapter II. Using this system, the densities of molecules on the plasma membrane were measured in HeLa cells expressing WT, M269R, R552G and R1131K. Positions of M269 and R552 are in the DH domain and HL between PH and REM domain, respectively (Fig. 3.2A) [Sondermann *et al.,* 2004]. R1131 is in G domain (Fig. 3.2B). Based on the crystal structure, NS mutation of SOS was classified into two classes by location of mutation [Lepri *et al.,* 2011]. M269R and R552G were classified in the class which reduces enzyme self-inhibition by conformational rearrangement. The residue of M269 interacted with REM domain directly and likely involved inhibition of interaction

between REM domain of SOS and RAS at allosteric site. R552G likely has abnormal interaction between H, DH and PH domains. Another class had a feature which enhances catalytic function of SOS by the membrane dependent mechanism and mutations in H and PH domains were classified in this class. And RAS activation at 15 min after EGF stimulation in the cells expressing M269R and R552G increased compared with WT SOS [Trataglia *et al.*, 2007]. R1131 is adjacent to S1132 which is phosphorylated by ERK.

The relative density of SOS molecules on the plasma membrane increased for all three NS mutants compared with that of WT (Fig. 3.3 left). This data indicates that NS mutants have a common feature in localization on the membrane. It is known that L687, R688 and W729 in SOS REM domain are essential for positive feedback response in RAS activation mediated by SOS [Margarit *et al.*, 2003]. By additional introduction of these triple mutations in REM domain into NS mutants, I examined the effect of interaction between REM domain and RAS on the dynamics of NS mutants on the membrane.

The membrane density of WT REM(-) before EGF stimulation was similar to that in WT (Fig. 3.3) . In the mutants of R552G REM(-) and R1131K REM(-), the densities before EGF stimulation were still high compared with the density in WT REM(-). On the other hand, the density before EGF stimulation in M269R significantly decreased. This result indicated that increase of the basal density in M269R was caused by REM/RAS interaction. In contrast, this interaction had no effect on the increase of density in R552G and R1131K. These data suggest that the contribution of REM/RAS interaction to the molecular density is different between the mutants.

### 3.3.2. Association with the plasma membrane in each NS mutants

The association rate constants between SOS molecules and the plasma membrane were measured in WT and NS mutants (Fig. 3.4A left). Method of the measurement in living cells was described in Chapter II. Compared with basal association rate constant in WT, those in M269R and R1131K were significantly high. On the other hand, that of R552G was similar to WT. In R1131K, basal level of association rate was still high without REM/RAS interaction but was significantly low in M269R (Fig. 3.4A right). Therefore the RAS/REM interaction affected association rate in M269R but didn't contribute to increase of association rate in R1131K. The relative association rate constant of dHR1131K, which is an H domain deletion mutant of R1131K, was the same level as that of R1131K (Fig. 3.4B). This result indicates that the association rate constant of mutated G domain ($G_{R1131K}$) to the membrane was high. The density of $G_{R1131K}$ was measured (Fig. 3.6). The density of $G_{R1131K}$ was approximately 1.5 times higher than WT G domain with EGF stimulation. Thus, it was suggested that the high density of $G_{R1131K}$ causes the high density of R1131K which was roughly 1.5 times higher than WT (Fig. 3.3 left). Before EGF stimulation, the density of GR1131K could not express high density of R1131K. It is unclear what causes the high density of R1131K.

### 3.3.3. Dissociation kinetics analysis of NS mutants from the membrane

Dwell time of SOS molecules on the plasma membrane was measured in the cells expressing M269R, R552G, R1131K and WT. Dwell time distribution in R552G and M269R without EGF stimulation was elongated from that of WT without

stimulation (Fig. 3.7AB left). In contrast to these mutants, the distribution of R1131K was similar to that of WT (Fig. 3.7C left). Based on the dissociation kinetics model of SOS from the plasma membrane proposed in Chapter II (Fig 3.7A left), the fraction of Intermediate (I) state was estimated. In the model, WT SOS molecules have three association states (H, G and I) on the plasma membrane. H and G are states in which either H or G domain interacts with the plasma membrane. In I state, both G and H domain interact with the plasma membrane simultaneously. It was suggested that the interaction with feedback RAS at REM domain occurs in only I state.

Based on the three states mode, the fraction of I state in NS mutants was compared with WT. In R552G, association rate constant in R552G was similar to that in WT (Fig. 3.4A). And it can be assumed that affinities of H and G domains in R552G are similar to that in WT. Thus, I assumed that R552G had two initial states and the ratio of initial states was similar to WT (Table 3.2A, B). In M269R, REM domain was involved in association of SOS with the plasma membrane (Fig. 3.4). In chapter II, there was an experimental result in which the dwell time distribution of REM(-) still shifted to the right at 3 min after EGF stimulation (Fig. 2.12). This data suggests that REM domain has high dissociation rates compared to that of G and H domains. So, in dissociation kinetics, dissociation of REM domain does not contribute to the dissociation of SOS molecules from the membrane. Thus, I assumed that REM domain in M269R affected association rate with the membrane and contributed to stabilization of I state on the membrane. I also presumed that the sum of association rate of G, H and REM domains could explain that of M269R, and determined the ratio of initial association state in M269R (Table. 3.2B). The level of association rate constant of R1131K without H domain was similar to R1131K (Fig.

3.4B). This result suggests that association of R1131K could be explained by that of $G_{R1131K}$. Thus, in R1131K, there was an initial state ($G_{R1131K}$) (Table 3.2). The dissociation constants were measured in truncated mutants (G, H, $G_{R1131K}$ ) (Table 3.1and Fig. 3.5). Under such conditions, population of Intermediate state (I state) was estimated in R552G, M269R and R1131K.

In M269R and R552G, population of I state increased in all periods measured in this experiment compared with WT (Fig. 3.7AB right). But, in R1131K, I state fractions were slightly changed from those of WT (Fig. 3.7C right). Without REM/RAS interaction, the fraction of I state significantly decreased in M269R but was still high in R552G. These data suggested that REM/RAS interaction contributed to increase of I state in M269R, but did not affect the fraction of I state in R552G. In R1131K, the contribution of REM/RAS interaction to the fraction of I state was the same level as that in WT.

### 3.3.4. Discussion

This study revealed that all of mutants used in this study resulted in common abnormal characteristics of high affinity for the plasma membrane (Fig. 3.3 left), but molecular mechanism leading to this high affinity was different.

In M269R, both fast association with and stabilization of I state caused high affinity for the plasma membrane (Table 3.3). And REM/RAS interaction contributed to both association and stabilization of I state (Fig. 3.4A, Fig. 3.7A). These data suggest that REM domain exposed by mutations associates with the plasma membrane directly. And SOS molecules have three initial association states in M269R (I, G and H), whereas WT SOS molecules have two initial association states

(G and H state) (Fig. 3.7A right, Fig. 3.8A). Because number of initial states in M269R is larger than WT, association rate with the plasma membrane increased compared to WT. Presence in large number of states on the plasma membrane caused increase of intermediate states (Fig. 3.7A left). Actually, in M269R, it is considered that association states other than I state are able to interact with feedback RAS by conformational change of SOS, resulting in abnormal SOS translocation. By this mechanism, it is suggested that the REM/RAS interaction is significantly affected in M269R and the positive feedback was greatly affected in M269R.

In R552G, only dissociation of SOS molecules from the membrane were repressed, leading to high affinity for the membrane (Table 3.3, Fig. 3.8B). These data suggests that the initial association states of R552G were similar to those of WT but high transition rates from G and H to I state resulted in increase of I state fraction (Fig. 3.7B right, Fig. 3.9). This data suggests that these high transition rates were caused by destabilization of autoinhibition conformation. Without interaction between H domain and helical linker, inhibition of REM domain by DH domain probably weakens, inducing exposure of REM domain easily. Thus, in R552G mutants, it is suggested that this destabilization of conformation causes the abnormal translocation of SOS. The destabilization did not involve the REM/RAS interaction because these transition rates were still high without REM/RAS interaction (Fig. 3.10). But in the presence of RAS-GTP, R552G probably mediates RAS positive feedback excessively.

In R1131K and R1131K REM(-), population of I state was similar to WT and WT REM(-), respectively (Fig. 3.7C right). But the association rate constants in both R1131K and R1131KREM were high compared with WT (Fig. 3.4A). The high

association with the membrane resulted in the excess translocation of R1131K. And high density of R1131K was caused by high density of $G_{R1131K}$ on the membrane after EGF stimulation (Fig. 3.6). Before stimulation, it is unclear what causes high density of R1131K. In dissociation kinetics analysis, transition rate of H to I state was high in R1131K compared with other NS mutants (Fig. 3.9). But, because there was slight H-state fraction (Fig. 3.11), the fraction of I state in R1131K was similar to WT. Thus, in R1131K, the high affinity of mutated G domain caused the abnormal SOS translocation. In R1131K, REM/RAS interaction did not affect localization of R1131K on the membrane. But, the increase of molecules which interacts with feedback RAS probably leads to increase of ensemble of SOS molecules on the membrane. The high association of R1131K was probably caused by inhibition of the ERK and RSK-mediated negative feedback. G domain of SOS is phosphorylated by ERK at S1132, S1167, S1193 and S1197 [Corbalan-Garcia *et al.,* 1996] (Fig. 1.5). The residue of R1131 is adjacent to S1132. And the residue of S1134 is phosphorylated by RSK [Saha *et al.,* 2012]. The minimal target motif of RSK includes the residue of R1131. So, there is a possibility that S1132 and S1134 in R1131K are not phosphorylated by ERK and RSK, inducing high affinity of G domain for Grb2 (Fig. 3.12). This possibility has to be confirmed by experiments using FCCS or pull down assay.

Finding of correlation between genotype and phenotype in NS was difficult. However, in SOS, it was reported that prevalence of fetal macrosomia in patients which have mutations in the class including M269R is significantly higher than that in patients in the class including R552G [Lepri *et al.,* 2011]. This report indicates that activation dynamics in RAS-MAPK pathway depends on the position of mutations in

SOS, inducing phenotypical difference in NS patients. Thus, there is a possibility that the difference in molecular mechanism which was identified in this study results in the phenotypical difference.

This study characterized the molecular mechanism of NS mutants in SOS from the view of SOS/RAS positive feedback by proposing a kinetic model. The study shows new possibility in which RAS activity can be controlled by modulation of the interaction between SOS domains or the affinity of G domain for the membrane. G domain probably has a role in regulating the affinity of SOS for the plasma membrane precisely. And this study also indicates that the interaction of H domain with helical linker functions as the stabilizer of SOS conformation. This stabilizer has a role which adequately maintains the fraction of I state, which binds to feedback RAS. In addition, the inhibition of REM domain caused by DH domain has a role to confine the interaction between SOS and feedback RAS to only the I state. When SOS has applicable affinity of G domain for the membrane, the switching of the SOS/RAS positive feedback by interaction of SOS domains might control RAS activation.

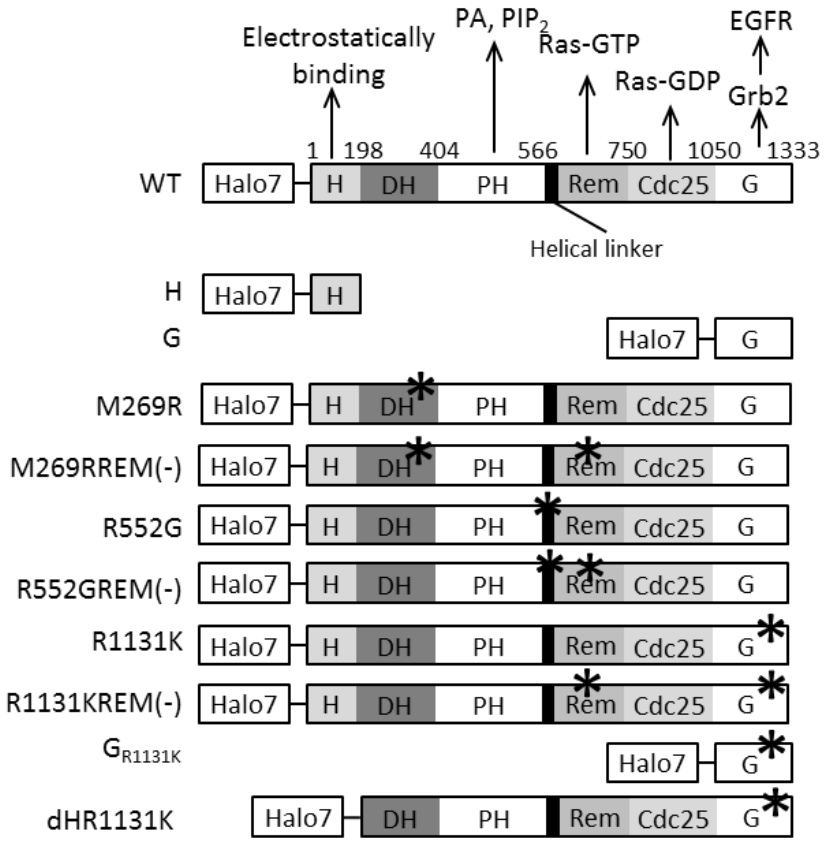


**Figure 3.1. Diagram of mutants used in this study**

SOS WT has five domains that interact independently with the membrane. M269, R552G and R1131K are located in DH domain, helical linker and G domain. Mutation in which positive feedback function is lost is shown as REM(-). dHR1131K is deletion mutant of H domain.

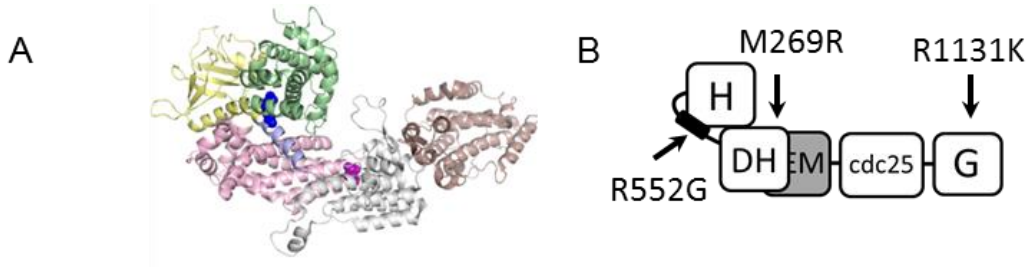


**Figure 3.2. Structure of SOS**

A) Crystal structure of SOS is shown. Blue and purple dots indicate position of R552 and M269. The ribbons shown as green, yellow, blue, magenta, gray, and wine red mean H, PH, helical linker, DH and Cdc25. G domain is located next to Cdc25. B) R1131K is located in G domain. DH domain inhibits interaction between REM domain and feedback RAS. Interaction between H domain and helical linker stabilizes autoinhibition of SOS. PH domain is not described in this diagram.

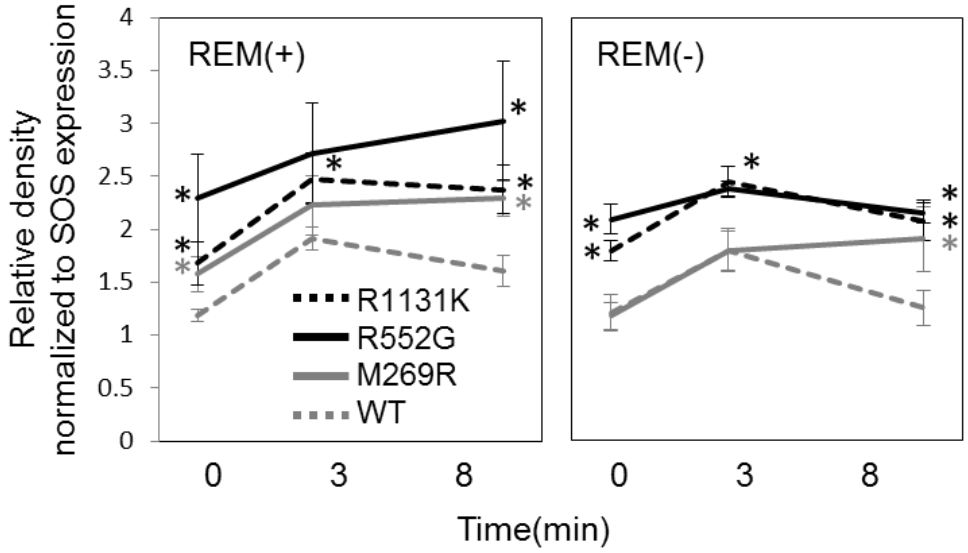


**Figure 3.3. Time course of density in WT and NS mutants on the plasma membrane with EGF stimulation**

Relative densities per unit area normalized to SOS expression level in single cell were shown. The density in WT, M269R, R552G and R1131K was shown as gray dotted line, gray line, black line and dotted black line. Right is REM(+) and left is REM(-). Asterisk is shown as comparison with WT, and means $p<0.05$ on Mann-Whitney test. Error bar means S.E.

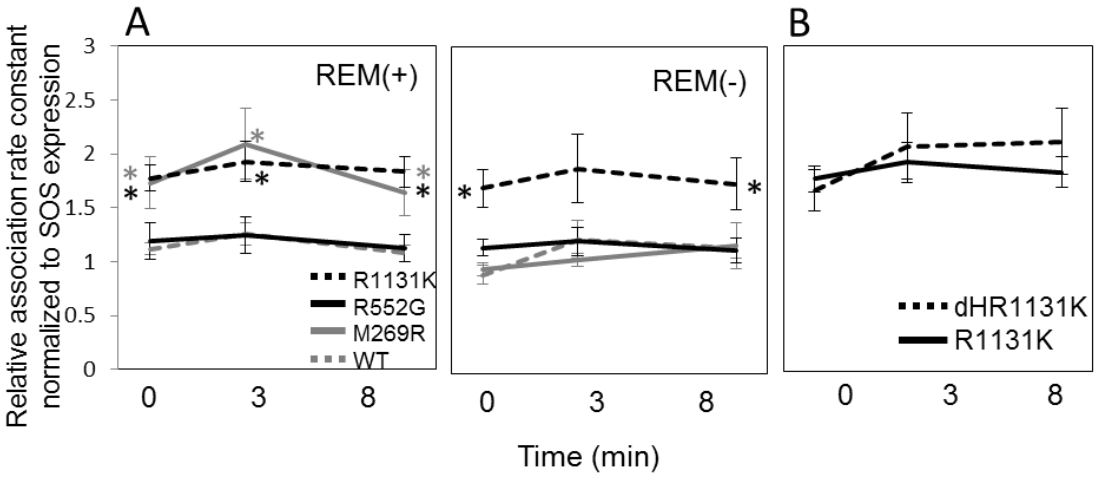


**Figure 3.4. Relative association rate constants of NS mutants, dR1131K and $G_{R1131K}$.** A) Relative association rate constants were normalized to SOS expression. The association rate constants in WT, M269R, R552G and R1131K were shown as gray dotted line, gray line, black line and dotted black line. NS mutants with and without REM/RAS interaction are shown as REM(+) and REM(-). B, C) Relative association rate constants of dHR1131K (B) and GR1131K (C) is shown. Error bar shows S.E. Asterisk shows $p<0.05$ on Mann-Whitney test.

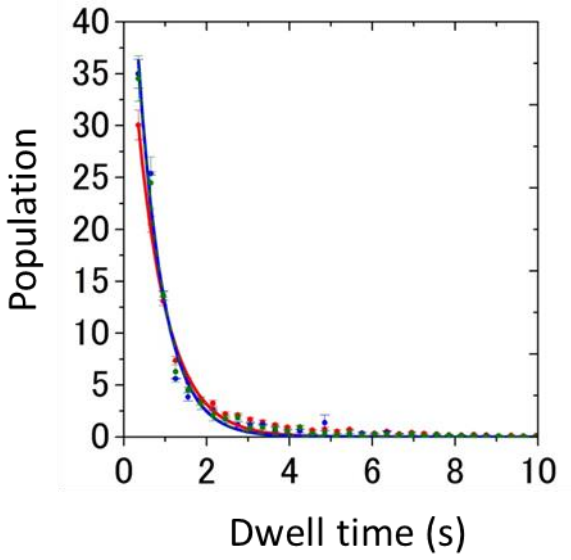


**Figure 3.5. Dwell time distribution of $G_{R1131K}$**

Experimental data without EGF stimulation and at 3 min and 8 min after stimulation were shown as blue, red and green dots. Blue, red and green solid lines mean fitting results without EGF and at 3 min and 8 min with EGF stimulation.

| | w/o EGF | 3min | 8min |
|---|---|---|---|
| H | 1.85 | 1.85 | 1.85 |
| G | 1.51 | 1.51 | 1.51 |
| $G_{R1131K}$ | 1.57 | 1.31 | 1.53 |

**Table 3.1. Dissociation rate constants of H, G and $G_{R1131K}$ domains**

Dissociation constant of H domain was higher than G domain every period. That of $G_{R1131K}$ was different between before and at 3 min after EGF stimulation.

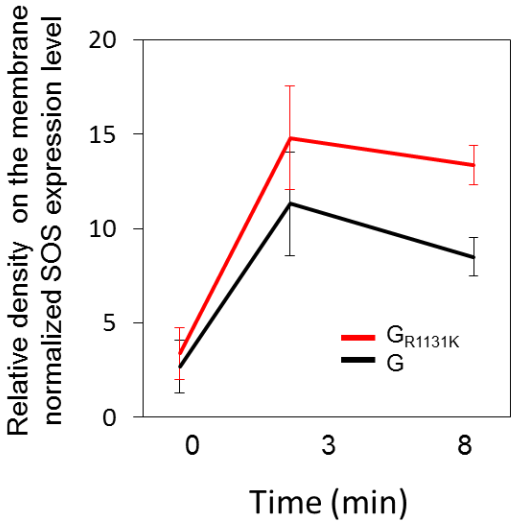


**Figure 3.6. Relative density on the membrane G and $G_{R1131K}$**

A) The relative density on the membrane of $G_{R1131K}$ and G domains were shown in red and blue line. After EGF stimulation, the density of $G_{R1131K}$ was 1.5 times higher than that of G. Before EGF stimulation, there was not significant difference between $G_{R1131K}$ and G.

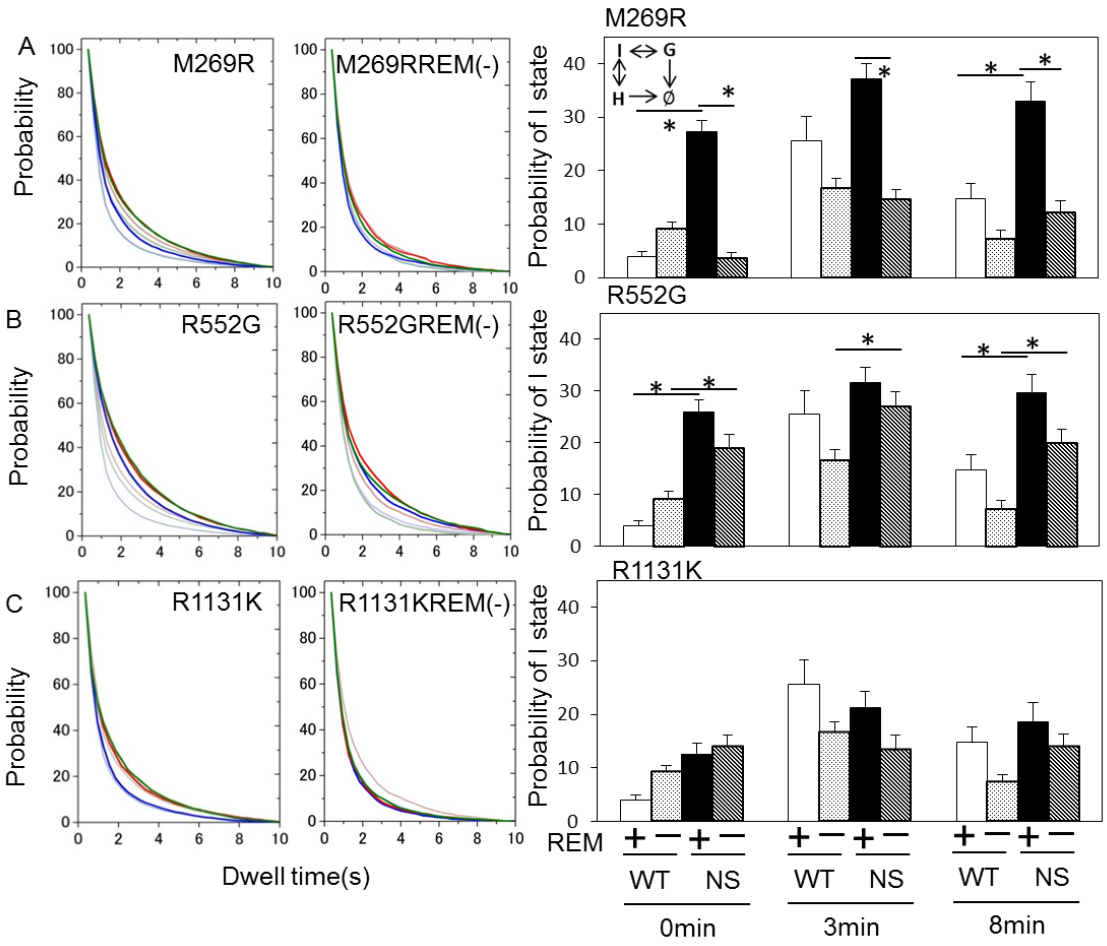


**Figure 3.7. Dwell time distribution and population of I state in NS mutants**

Dwell time distributions of M269R (A), R552G (B) and R1131K (C) are shown before (blue) and after 3 min (red) and 8 min (green) with EGF stimulation (left). Dwell time distributions of WT SOS before (blue) and at 3 min (red) and 8 min (green) EGF stimulation are shown as thin line. By using three states kinetic model (M269R inset), the fraction of I state was estimated from dwell time distribution of single cell. Asterisk means $p<0.05$ which was estimated by comparison with WT.

A

| | | | |
|---|---|---|---|
| M269R | H | G | I |
| R552G | H | G | |
| R1131K | | $G_{R1131K}$ | |

B

| | w/o EGF | | | 3min | | | 8min | | |
|---|---|---|---|---|---|---|---|---|---|
| | G | H | I | G | H | I | G | H | I |
| M269R | 0.4 | 0.2 | 0.4 | 0.5 | 0.1 | 0.4 | 0.5 | 0.2 | 0.3 |
| R552G | 0.7 | 0.3 | 0 | 0.8 | 0.2 | 0 | 0.7 | 0.3 | 0 |
| R1131K | 1 | 0 | 0 | 1 | 0 | 0 | 1 | 0 | 0 |

**Table 3.2. Initial association state and ratio of initial state in NS mutants**

A) There were three and two initial association states in M269R and R552G. In R1131K, the initial state was only $G_{R1131K}$. B) The ratio of initial states are shown.

| | Density | On-rate | I state |
|---|---|---|---|
| M269R | High | High | High |
| R552G | High | Same level | High |
| R1131K | High | High | Same level |

**Table 3.3. Brief description of abnormal molecular dynamics on the plasma membrane in NS mutants by comparison with WT**

In M269R, it was shown that excess translocation was derived from both association and dissociation. High density in R552G was caused by increase of I state. In R1131K, high association of $G_{R1131K}$ caused high translocation on the membrane.

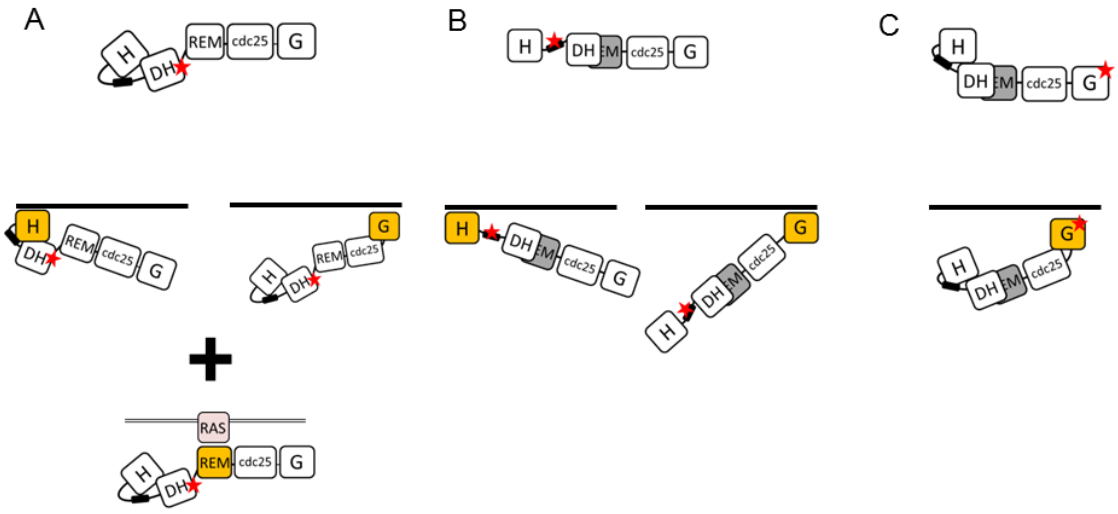


**Figure 3.8. Proposed molecular mechanism in NS mutants**

A) There were three initial association states in M269R. The state in which REM domain directly interacted with feedback RAS was specific to M269R. Because REM domain had high dissociation and low association rate constants, dissociation model was able to be simplified. B) In R552G, initial state was same as WT. But transition rate to I-state was high compared with WT. C) High affinity of $G_{R1131K}$ domain for the membrane caused excess translocation in R1131K. Conformation of SOS in R1131K was similar to WT.

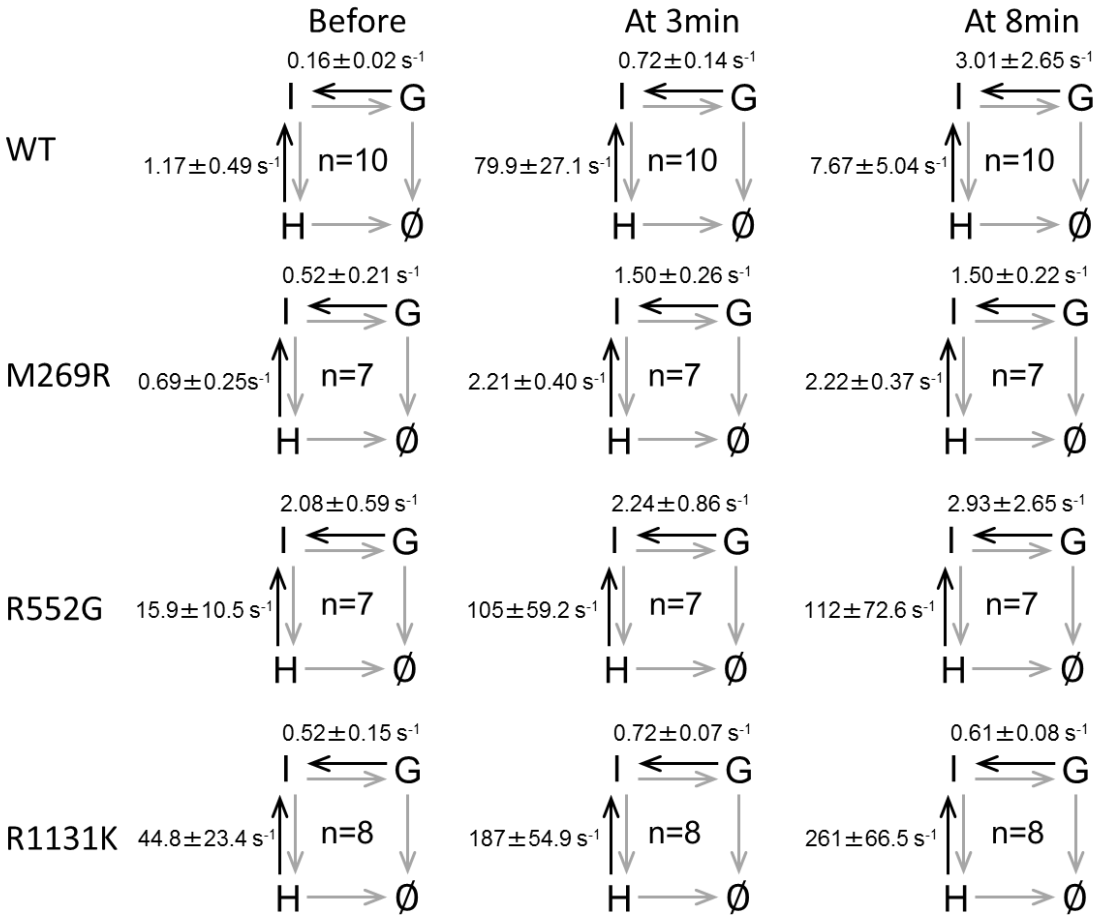


**Figure 3.9. Estimated transition rate in WT and NS mutants**

Transition rate from G to I ($k_{1r}$) and from H to I ($k_{2r}$) in WT and NS mutants is shown. In R1131K, although transition rate of H to I was high, the fraction of H state was quite low. So the fraction of I state in R1131K was same level as WT.

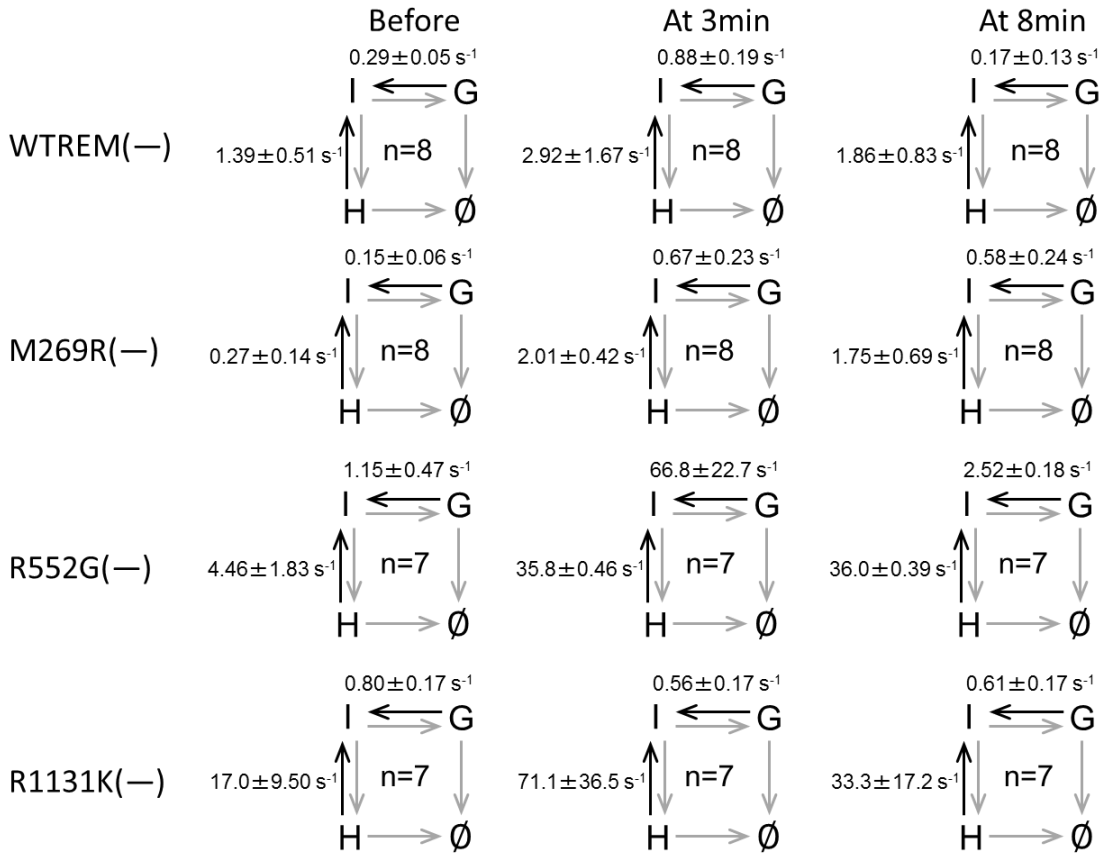


**Figure 3.10. Transition rate in WTREM(–) and NS REM(–)**

Transition rates from G to I ($k_{1r}$) and from H to I ($k_{2r}$) are shown in WT REM(–) and NS REM(–) mutants. The values of k1r and k2r in M269R REM(–) were same compared with that in WT. On the other hand, in R552G REM(–), these values were still high without RREM/RAS interaction.

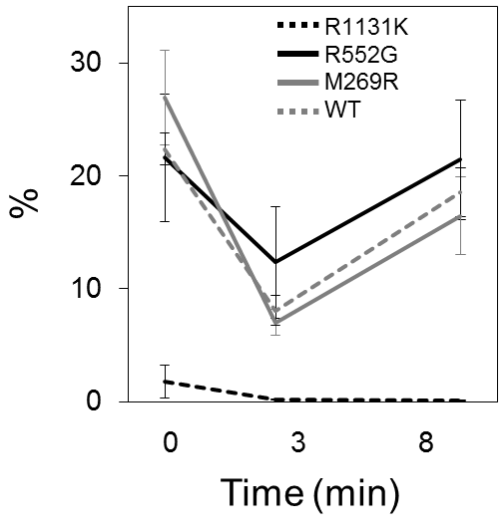


**Figure 3.11. Population of H state in NS mutants and WT**

Time course of H state in R1131K (dotted black line), R552G (solid black line), M269R (solid gray line) and WT (dotted gray line) are shown. H state of R1131K was quite low compared with other NS mutants and WT.

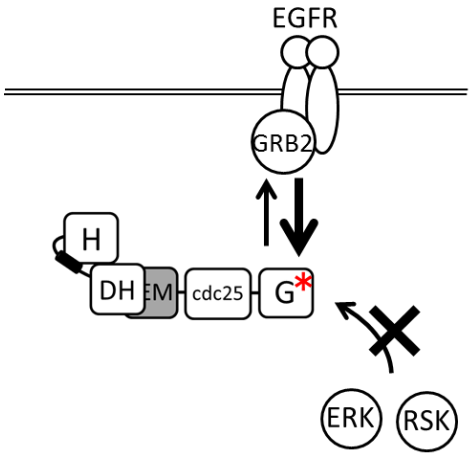


**Figure 3.12. Molecular mechanism which causes abnormal increase of density in R1131K**

Because R1131K inhibits phosphorylation at S1132 and S1134 by ERK and RSK, G domain might interact with Grb2 strongly. This molecular mechanism leads to high affinity for the membrane in R1131K.

# Chapter IV

## 4. Conclusion and Future direction

## 4.1. Conclusion

To understand signal dependent cell response, the activation mechanism of RAS, which is one of hub protein has to be clarified. Characterization of particular RAS activation mechanism in living cells leads to the basal therapy of NS, in which there is correlation between phenotypes and mutation. Thus, clarification of RAS activation mechanism is significant for cell biology and medical attention. SOS, which is a RAS guanine nucleotide exchange factor, controls RAS activity depending on EGF stimulation, leading to regulation of cell proliferation, differentiation and survival. So, SOS is an important protein to direct cell fate. The main purpose in this study is understanding of RAS activation mechanism caused by SOS. To arrive at this main purpose, I focused on the identification of the mechanism of SOS mediated-RAS positive feedback, which was crucial for RAS activation. I examined the dynamics of SOS closely on the plasma membrane in living cells. Detection of SOS molecules on the membrane had been difficult, because SOS molecules mainly exist in the cytosol and there are few molecules on the membrane. So, by using single molecule analysis in living cells, I examined the dynamics of SOS in living cells and proposed a dissociation kinetics model of SOS.

In Chapter II, it became clear that the SOS/RAS positive feedback causes sustainment of intermediate (I) state and elongation of molecular dwell time on the plasma membrane, inducing localization of SOS molecules on the plasma membrane at the later stage. And it was suggested that positive feedback functions in living cells and is required for signal dependent RAS activation. Additionally, abnormal orientation of H domain caused disappearance of RAS activation with EGF signal.

These results suggest that not only activated-RAS but also concerted interaction of SOS domains regulates SOS/RAS positive feedback.

These results suggest that abnormal interaction with SOS domains causes increase and decrease of RAS activity. In Chapter III, I used SOS mutants resulting in Noonan syndrome as gain of function mutants. Mutations of SOS identified in patients with NS are located in various SOS domains. Mainly these mutations exist not ~~only~~ in the catalytic domain but in the H, helical linker, DH and G domain. These data suggest that NS mutation is caused by abnormal interaction of SOS domains, supporting my hypothesis that abnormal interactions between SOS domains cause excess RAS activity. So, I examined the dynamics of SOS NS mutation in living cells, by using the SOS kinetic model. My data showed that the NS mutants used in this study have a common feature that is the high translocation to the plasma membrane, but the molecular mechanism resulting in the high-translocation varied between three mutants. By the analysis of M269R, it was indicated that an abnormal conformation in which REM domain is exposed caused the excess association with the membrane and the increase in the number of molecules interacting with feedback RAS. So, this mutation might significantly affect SOS/RAS positive feedback. In R552G, destabilization of autoinhibition led to transition to the intermediate state, inducing excess RAS positive feedback. This mutation might enhance the positive feedback mildly, compared with M269R. The result of AI(-) mutated at D140A (Fig. 2.1, 2.5) was different to the result of R552G. This distinction was probably caused by different interaction between H domain and HL. R552 in HL interacts with D140 and K169 in H domain (Fig. 4.1). In D140A mutant, R552 could interact with K169. This defective interaction probably inhibited the transition to intermediate state. On the

other hand, this interaction was completely lost in R552G, inducing an increased transition to the intermediate state. Thus, it is suggested that precise regulation of the interaction between H domain and HL is essential for normal SOS activity. Then, a feature of R1131K was identified, in which an increase in the high density of mutated G domain within the plasma membrane caused high translocation of SOS (Fig. 3.4B and Fig. 3.6). It was suggested that R1131K has effect on the positive feedback similarly to WT. Thus, this study identified the difference of the molecular mechanism in these mutants which cause abnormal SOS dynamics from the view of SOS/RAS positive feedback.

For the Noonan syndrome's therapy, this result suggests a novel probability that RAS activation is modulated by altering the interaction between SOS domains or the affinity of particular domain for the plasma membrane. In a previous study, the prevalence of fetal macrosomia in patients in the class including M269R was higher than that in the class including R552G [Lepri *et al.*, 2011]. The patients with M269R might have severe phenotype compared to those with R552G because M269R enhances the SOS/RAS positive feedback more significantly than R552G.

Additionally, my study suggests that the SOS dynamics on the membrane is regulated by the interaction between domains in SOS and the affinity of G domain for the membrane. Although the I state fraction of R1131K was not significantly different from that of WT, it is known that R1131K causes Noonan syndrome. This shows the possibility that SOS/RAS positive feedback controls RAS activation only when SOS has adequate affinity for the membrane. This study also suggests that switching of SOS/RAS positive feedback is regulated by interaction between SOS domains in living cells and SOS functions as a positive feedback regulator of RAS in living cells.

There is a possibility that because the affinity of G domain with the plasma membrane is crucial for normal SOS dynamics, G domain is regulated by multiple proteins like ERK and RSK. In addition to ERK and RSK, in cells, proteins which bind to various domain of SOS exist such as ezrin (PH), CIIA (PH), 14-3-3 (G) and P32 (DH) [Geißlera *et al.,* 2013; Hwang *et al.,* 2011; Saha *et al.*, 2012; Miura *et al.*, 2001]. It is possible that association of these proteins with SOS might modulate the interaction between SOS domains and regulate SOS/RAS positive feedback, regulating RAS activation in living cells.

## 4.2. Future direction and outlook

This study revealed that there are different molecular mechanisms in each NS mutant. So, to resume normal SOS dynamics, target interaction which has to be repressed might be different in each mutant. In previous studies, the small molecules which control the interaction between SOS catalytic site and RAS were identified [Burns *et al.,* 2014; Leshchiner *et al.,* 2015]. But, the pharmacologic treatment for NS by using this small molecule might result in mutation dependent-side effects, because molecular mechanism causing increase of RAS activation is different in each mutation. I suggest that molecular mechanism causing RAS activation has to be characterized, and normal RAS activation dynamics has to be assumed in living cells. This approach might lead to the development of a therapy without side effects.

SOS interacts with various proteins in living cells. And this study shows that there is a possibility that binding of SOS to partner protein alters the RAS positive

feedback response in normal living cells. In future studies, I will examine whether the other proteins which binds to SOS regulates SOS/RAS positive feedback.

In the analysis of NS mutants, it was suggested that excess translocation of R1131K is caused by high affinity of $G_{R1131K}$ in which interaction with Grb2 was promoted. To confirm this hypothesis, I have to examine whether complex of $G_{R1131K}$ and Grb2 increases compared with WT or not. This experiment will be performed by using Fluorescence cross-correlation spectroscopy (FCCS) and pull down assay.

This study also revealed the various molecular mechanisms between NS mutants. But it is still unclear whether these mechanisms induce different RAS activation dynamics. Therefore RAS activation dynamics has to be measured in living cells.

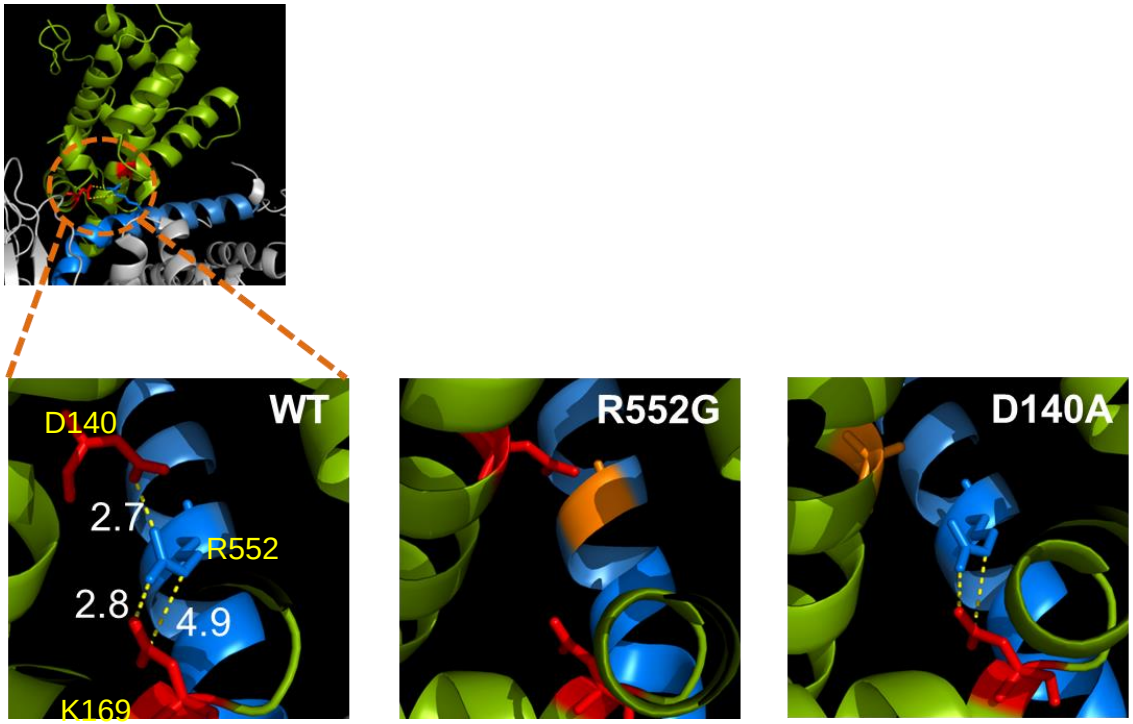


**Figure 4.1 structure of interaction between H domain and helical linker**

Green ribbon and blue ribbon show H domain and helical linker in SOS. The residues of D140, K169 and R552 are shown as red and blue sticks. D140 and K169 in H domain interact with R552 in helical linker. In R552G mutant, the interaction is completely lost. But, in D140A mutant, there is still the interaction between K169 and R552.

## 5, Acknowledgement

I would like to express my sincere gratitude to my supervisor, Chief Scientist Yasushi Sako Ph.D. (cellular informatics laboratory, RIKEN) and Director Toshio Yanagida Ph.D. ( Nanobiology Laboratories, Graduate School of Frontier Biosciences, Osaka University). I wish to express my warm thanks to Professor Masaru Ishii Ph.D., Professor Keiichi Namba Ph.D., Professor Yasushi Inoue Ph.D. (Graduate School of Frontier Biosciences, Osaka University) and Professor Masahiro Ueda Ph.D. (Department of Biological Sciences, Graduate School of Science, Osaka University) for evaluating my work. I thank Dafna Bar-Sagi, at New York University School of Medicine for the pCGM-HA-hSos1 plasmid. And I wish to express my sincere thanks to Kayo Hibino Ph.D. (Biological Macromolecules Laboratory, Structural Biology Center, National Institute of Genetics) for her help in the single molecule analysis and in the aspect of biochemical framework. I thank Ms. Hiromi Sato for technical assistance in construction of plasmids used in this study. I also thank cellular informatics Laboratory members for precious discussions and optical technical supports. And I thank Ms. Eri Taniguchi and Yu Yamada (administration staff at Nanobiology Laboratories) for their help in office procedure.

Here, I would like to express my deep gratitude to my parents, Saki and Kinako.

My work is supported by a Junior Research Associate (JRA) grant from RIKEN.

Yuki Nakamura

## 6, Reference

Allason J. E., Hall N.G., Hughes H.E., Preus M. & Witt R. D. Noonan syndrome: the changing phenotype. Am. J. Med. Genet. 21, 507-514 (1985).

Aronheim, A., Engeliberg, D., Li, N., Al-Alawi, N., Schlessinger, J. & Karin, M. Membrane targeting of the nucleotide exchange factor Sos is sufficient for activating the Ras signaling pathway. Cell 78, 949–961 (1994).

Boguski M. S. & Mccormick F. Proteins regulating Ras and its relatives. Nature 366, 643-654 (1993).

Boriack-Sjodin, P. A., Margarit, S. M., Bar-sagi, D. & Kuriyan, J. The structural basis of the activation of Ras by Sos. Nature 394, 337–343 (1998).

Burns M. C., Sun Q., Daniels R. N., Camper D., Kennedy J. P., Phan J., Olejniczak E. T., Lee T., Waterson A. G., Rossanese O. W. & Fesik S. W. Approach for targeting Ras with small molecules that activate SOS-mediated nucleotide exchange. Proc. Natl. Acad. Sci. USA 111, 3401-3406 (2014).

Chardin, P., Camonis, J. H., Gale, N. W., Aelst, L. V., Schlessingler, J., Wingler, M. H., et al. Human Sos1; a guanine nucleotide exchange factor for Ras that binds to GRB2. Science 260, 1338–1343 (1993).

Chen P. C., Wakimoto H., Conner D., Araki T., Yuan T., Roberts A.,Seidman C. E., Bronson R., Neel B. G., Seidman J.G.& Kucherlapati R. Activation of multiple signaling pathways causes developmental defects in mice with a Noonan syndrome-associated Sos1 mutation. J. Clin. Invest. 120, 4353-4365 (2010).

Chen, R.-H., Corbalan-Garcia, S. & Bar-Sagi, D. The role of the PH domain in the signal-dependent membrane targeting of Sos. EMBO J. 16,1351–1359 (1997).

Corbalan-Garcia, S., Yang, S. S., Degenhardt K. R. & Bar-Sagi, D. Identification of the mitogen-activated protein kinase phosphorylation sites on human Sos1 that regulate interaction with Grb2. Mol. Cell Biol. 16, 5674–5682 (1996).

Das, J., Ho, M., Zikherman, J., Govern, C., Yang, M., Weiss, A., Chakraborty, A. K. & Roose, J. P. Digital signaling and hysteresis characterize Ras activation in lymphoid cells. Cell 136:337–351 (2009).

Der C. J., Krontiris T. G. & Cooper G. M. Transforming genes of human bladder and lung carcinoma cell lines are homologous to the ras genes of Harvey and Kirsten sarcoma viruses. Proc. Natl Acad. Sci. USA. 79, 3637–3640 (1982).

Geißlera K. J., Junga M. J., Rieckena L. B., Sperkab T., Cuia Y., Schackea S., Merkela U., Markwartc R., Rubioc I., Thand M. E., Breithaupte C., Peukerf S., Seifertf R., Kauppf U.B., Herrlichb P. & Morrisona H. Regulation of Son of sevenless

by the membrane-actin linker protein ezrin. Proc. Natl. Acad. Sci. USA 110, 20587-20592 (2013)

Gureasko, J., Kuchment, O., Makino, D. L., Sondermann, H., Bar-Sagi, D. & Kuriyan, J. Role of the histone domain in the autoinhibition and activation of the Ras activator Son of Sevenless. Proc. Natl. Acad. Sci. USA 107, 3430–3435 (2010).

Hall B. E., Yang S. S., Boriack-Sjodin P. A., Kuriyan J. & Bar-Sag D. Structure-based Mutagenesis Reveals Distinct Functions for Ras Switch 1 and Switch 2 in Sos-catalyzed Guanine Nucleotide Exchange. J. Biol. Chem. 276, 27629-27637 (2001).

Harvey J. J. An Unidentified Virus which causes the Rapid Production of Tumours in Mice. Nature 204, 1104-1105 (1964).

Heldin C. H. Dimerization of Cell Surface Receptors in Signal Transduction. Cell 80, 213-223 (1995).

Hibino, K., Hiroshima, M., Takahashi, M. & Sako, Y. Single-molecule imaging of fluorescent proteins expressed in living cells. Methods Mol. Biol. 48, 451–460 (2009).

Hibino, K., Shibata, T., Yanagida, T. & Sako, T. Ativation kinetics of RAF protein in the ternary complex of RAF, RAS-GTP, and kinase on the plasma membrane of living cells. J. Biol. Chem. 286, 36460–36468 (2011).

Hibino, K., Watanabe, T. M., Kozuka, J., Hikikoshi Iwane, A., Okada, T., Kanaoka, T., Yanagida, T. & Sako, Y. Single- and multiple-molecule dynamics of the signaling from H-Ras to cRaf-1 visualized on the plasma membrane of living cells. *ChemPhysChem* **4**, 748–753 (2003).

Hiroshima, M., Saeki, Y., Okada-Hatakeyama, M. & Sako, Y. Dynamically varying interactions between heregulinand ErbB proteins detected by single-molecule analysis in living cells. Proc. Natl. Acad. Sci. USA 109, 13984–13989 (2012).

Hwang H.S., Hwang S. G., Cho J. H., Chae J. S., Yoon K. W., Cho S. G. & Choi E .J. CIIA functions as a molecular switch for the Rac1-specific GEF activity of SOS1. JCB 195, 377-386 (2011)

Iversen, L., Tu, H., Lin, W., Cristensen, S. M., Abel, S. M., Iwig, J., Wu, H., Gureasko, J., Rhodes, C., Petit, R. S., Hansen, S. D., Thill, P., Yu, C.-H., Stamou, D., Chakraborty, A. K., Kuriyan, J. & Groves, J. T. Ras activation by SOS: allosteric regulation by altered fluctuation dynamics. Science 345, 50–54 (2014).

Jaqaman, K., Loerke, D., Mettle, M., Kuwata, H., Grinstein, S., Schmid, S. L. & Danuser, G. Robust single-particle tracking in live-cell time-lapse sequences. Nat. Methods 5, 695–702 (2008).

Karnoub A. E & Weinberg R. A. Ras oncogenes: split personalities. Mol. Cell Biol. 9, 517-531 (2008).

Kirsten W. H. & Mayer L. A. Morphologic responses to a murine erythroblastosis virus. Natl Cancer inst 39, 311-35 (1967).

Leevers, S. J., Paterson, H. F. & Marshall, C. J. Requirement for Ras in Raf activation is overcome by targeting Raf to the plasma membrane. Nature 369, 411–414 (1994).

Lepri, F., Luca, A. D., Stella, L., Rossi, C., Baldassarre, G., Pantaleoni, G., et al. SOS1 mutations in Noonan syndrome: molecular spectrum, structural insights on pathogenic effects, and genotype–phenotype correlation. Hum. Mutat. 32, 760–772 (2011)

Leshchiner E. S., Parkhitko A, Bird G.H., Luccarelli J., Bellairs J. A., Escudero S., Opoku-Nsiah K., Godes M., Perrimon N. & Walensky L.D. Direct inhibition of oncogenic KRAS by hydrocarbon-stapled SOS1 helices. Proc. Natl. Acad. Sci. USA 112, 1761-1766 (2015)

Margarit, S. M., Sondermann, H., Hall, B. E., Nagar, B., Hoelz, A., Pirruccello, M., Bar-Sagi, D. & Kuriyan, J. Structural evidence for feedback activation by Ras·GTP of the Ras-specific nucleotide exchange factor SOS. Cell 112, 685–695 (2003).

Matsuoka, S., Iijima, M., Watanabe, T., Kuwayama, H., Yanagida, T., Devreotes, P. N. & Ueda, M. Single-molecule analysis of chemoattractant-stimulated membrane recruitment of a PH-domain-containing protein. J. Cell Sci. 119, 1071–1079 (2006).

Mendez H. M. M. & Opitz J. M. Noonan syndrome: A Review. Am. J. Med. Genet. 21, 493-506 (1985).

Milburn, M. V., Tong, L., Devos, A. M., Brüger, A., Ymaizumi, Z., Nishimura, S., et al. Molecular switch for signal transduction: structural differences between active and inactive forms of protooncogenic ras proteins. Science 247, 939–945 (1990).

Miura K., Miyazawa S., Furuta S., Mitsushita J., Kamijo K., Ishida H., Miki T., Suzukawa K., ResauJ., CopelandT. D. & Kamata T. The Sos1-Rac1 Signaling. J. Biol. Chem. 276, 46276-46283 (2001).

Narumi Y. et al. Clinical manifestations in patients with SOS1 mutations range from Noonan syndrome to CFC syndrome. J. Hum. Genet. 53, 834–841 (2008).

Oda K, Matsuoka Y, Funahashi A & Kitano H. A comprehensive pathway map of epidermal growth factor receptor signaling. Mol. Syst. Biol. 1, 1-17 (2005).

Olayioye, M. A., Neve, R. M., Lane, H. A. & Hynes, N. E. The ErbB signaling network: receptor heterodimerization in development and cancer. EMBO J. 19, 3159–3167 (2000).

Quilliam, L. A., Huff, S. Y., Rabun, K. M., Wei, W., Park, W., Broek, D. & Der, C. J. Membrane-targeting potentiates guanine nucleotide exchange factor CDC25 and SOS1 activation of Ras transforming activity. Proc. Natl. Acad. Sci. USA 91, 8512-8516 (1994).

Parada L. F., Tabin C. J., Shi C. & Weinberg R. A.Human EJ bladder carcinoma oncogene is homologue of Harvey sarcoma virus ras gene. Nature 297, 474–478 (1982).

Reddy E. P., Reynolds R. K., Santos E. & Barbacid M. A point mutation is responsible for the acquisition of transforming properties by the T24 human bladder carcinoma oncogene. Nature 300, 149-152 (1982).

Roberts A. E., Araki T., Swanson K. D., Montgomery K. T., Schiripo T. A., Joshi V. A., Li L., Yassin Y., Tamburino A. M., Neel B. G. & Kucherlapati R. S. Germline gain-of-function mutations in SOS1 cause Noonan syndrome. Nat. Genet. 39, 70-74 (2007).

Saha M, Carriere A, Cheerathodi M, Zhang X, Lavoie G. E., Rush J., Roux P. P. & Ballif B.A. RSK phosphorylates SOS1 creating 14-3-3-docking sites and negatively regulating MAPK activation. Biochem. J. 447, 159–166 (2012).

Santos E., Tronick S. R., Aaronson S. A., Pulciani S. & Barbacid M. T24 human bladder carcinoma oncogene is an activated form of the normal human homologue of BALB- and Harvey-MSV transforming genes. Nature 298, 343–347 (1982).

Shimizu K., Goldfarb M., Perucho M. & Wiglert M. Isolation and preliminary characterization of the transforming gene of a human neuroblastoma cell line. Proc. Natl Acad. Sci. USA. 80, 383-387 (1983).

Simon, M. A., Bowtell, D. D., Dodson, G. S., Laverty, T. R. & Rubin, G. M. Ras1 and a putative guanine nucleotide exchange factor perform crucial steps in signaling by the sevenless protein tyrosine kinase. Cell 67, 701–716 (1991).

Sondermann, H., Nagar, B., Bar-Sagi, D. & Kuriyan, J. Computational docking and solution x-ray scattering predict a membrane-interacting role for the histone domain of the Ras activator son of sevenless. Proc. Natl. Acad. Sci. USA. 102, 16632–16637 (2005).

Sondermann, H., Soisson, S. M., Bar-Sagi D. & Kuriyan, J. Tandem histone folds in the structure of the N-terminal segment of the Ras activator Son of Sevenless. Structure 11, 1583–1593 (2003).

Sondermann, H., Soisson, S. M., Boykevisch, S., Yang, S.-S, Bar-Sagi, D. & Kuriyan, J. Structural analysis of autoinhibition in the Ras activator Son of sevenless. Cell 199, 393–405 (2004).

Stokoe, D., Macdonald, S. G., Cadwallader, K., Symons, M. & Hancock, J. F. Activation of Raf as a result of recruitment to the plasma membrane. Science 264, 1463–1467 (1994).

Tartaglia M. and Gelb, B.D. Noonan syndrome and related disorders: genetics and pathogenesis. Annu. Rev. Genomics Hum. Genet. 6, 45–68 (2005).

Tartaglia M. et al. Gain-of-function SOS1 mutations cause a distinctive form of Noonan syndrome. Nat. Genet. 39, 75-79 (2007).

Vojtek A. B. & Der C. J. Increasing Complexity of the Ras Signaling Pathway. J. Biol. Chem 273, 19925–19928 (1998).

Yadav, K. K. & Bar-Sagi, D. Allosteric gating of Son of sevenless activity by the histone domain. Proc. Natl. Acad. Sci. USA 107, 3436–3440 (2010).

Weiss A. & Schlessinger J. Switching Signals On or Off by Receptor Dimerization. Cell 94, 277–280 (1998).

Yang, S., Aelst, L. V. & Bar-Sagi, D. Differential interactions of human Sos1 and Sos2 with Grb2. J. Biol. Chem. 270, 18212–18215 (1995).

Z Natasha, J. L. Oliva, N. Martínez, R. Jorge, A Ballester, S. G-Eisman, S G-Vargas, and J. M. Rojas. Grb2 is a negative modulator of the intrinsic Ras-GEF activity of

hSos1. Mol. Biol. Cell. 17, 3591-3597 (2006).

Zenker M, Rowe S. L, Böll S, Klein C, Bollag G., van der Burgt I., Musante L, Kalscheuer V., Wehner L. E., Nguyen H., West B., Zhang K. Y. J., Sistermans E., Rauch A., Niemeyer C. M., Shannon K. & Kratz C. P. Germline KRAS mutations cause Noonan syndrome. Nat. Genet. 38, 331–336 (2006).

Zhao, C., Du, G., Skowronek, K., Frohman, M. A. & Bar-Sagi, D. Phospholipase D2-generated phosphatidic acidcouples EGFR stimulation to Ras activation by Sos. Nat. Cell Biol. 9, 706–712 (2007).

## 7, Publication list

・学術誌等

① Yuki Nakamura, Kayo, Hibino, Toshio Yanagida and Yasushi Sako

Switching of the positive feedback for RAS activation by a concerted function of SOS membrane association domains. Biophysics and phisicobiology, 13, 1-11. 2016)

② Yuki Nakamura, Kayo, Hibino, Toshio Yanagida and Yasushi Sako

Classification of molecular dynamics in SOS Noonan syndrome mutants from the properties of SOS-mediated RAS positive feedback. (in prep).

③ Kayo Hibino, Michio Hiroshima, Yuki Nakamura, and Yasushi Sako.

Single-molecule imaging measurements of protein-protein interactions in living cells. "An Integrated View of the Molecular Recognition and Toxinology – From Analytical Procedures to Biomedical Applications" InTech. pp433-453. 2013

・学会・シンポジウム等における発表

① ○Yuki Nakamura, Kayo Hibino, Yasushi Sako

Single molecule imaging of guanine nucleotide exchange factor Sos in living cells.

日本生物物理学会第 50 回年会、名古屋大学、2012 年 9 月(口頭)

② ○中村由樹、日比野佳代、佐甲靖志

「グアニンヌクレオチド交換因子 Sos の細胞内一分子計測」

定量生物の会第 5 回年会、東京大学駒場 II キャンパス生産技術研究所、2012 年 11 月(ポスター)

③ ○中村由樹、日比野佳代、佐甲靖志
「RasGTP/GDP 交換因子 Sos の一分子解析による Ras/Sos positive feedback 機構の解明」
理研シンポジウム「細胞システムの動態と論理 IV」、理化学研究所、2013 年 3 月(口頭、ポスター)

④ ○中村由樹、日比野佳代、佐甲靖志
「RasGTP/GDP 交換因子 Sos の一分子解析を用いた Ras/Sos positive feedback 機構の解明」
第二回生物物理学会関東支部会、東京農工大学、2013 年 4 月口頭)

⑤ ○Yuki Nakamura, Kayo Hibino, Yasushi Sako
Positive feedback regulation of SOS-mediated Ras activation detected by single-molecule analysis in living cells
日本生物物理学会第 51 回年会、国立京都国際会館、2013 年 10 月(ポスター)

⑥ ○中村由樹、日比野佳代、佐甲靖志
RasGTP/GDP 交換因子 Sos の一分子解析による Ras/Sos positive feedback 機構の解明
理研シンポジウム「細胞システムの動態と論理 V」、理化学研究所、2014 年 3 月(ポスター)

⑦ ○Yuki Nakamura, Kayo Hibino, Yasushi Sako

Dysregulations of SOS-mediated positive feedback on RAS activation in Noonan syndrome observed using single molecule imaging

日本生物物理学会第 52 回年会、札幌コンベンションセンター、2014 年 9 月(ポスター)

⑧ ○Yuki Nakamura, Kayo Hibino, Yasushi Sako

Dysregulations of the SOS-RAS feedback analyzed in single molecules of Noonan syndrome mutants of SOS

第 37 回日本分子生物学会年会　パシフィコ横浜　2014 年 11 月(ポスター)

⑨ ○中村由樹、日比野佳代、佐甲靖志

Noonan 症候群における SOS/RAS positive feedback 異常制御の生細胞一分子解析

理研シンポジウム「細胞システムの動態と論理Ⅶ」、理化学研究所、2015 年 4 月(ポスター)

⑩ ○Yuki Nakamura, Kayo Hibino, Yasushi Sako

Classification of molecular dynamics in SOS Noonan syndrome mutants from the properties of SOS-mediated RAS positive feedback

日本生物物理学会第 53 回年会、金沢大学角間キャンパス、2015 年 9 月(ポスター)

**・招待講演**

○中村由樹、日比野佳代、佐甲靖志

Noonan 症候群における SOS を介した RAS positive feedback 異常制御の生細胞一分子解析

研究会「理論と実験」、広島大学東広島キャンパス、2014 年 10 月(口頭)